Journal of Anatomy

J. Anat. (2013) doi: 10.1111/joa.12108

Comparative study of notoungulate (Placentalia, Mammalia) bony labyrinths and new phylogenetically informative inner ear characters

Thomas E. Macrini,[1,2] John J. Flynn,[2,3] Xijun Ni,[2,4] Darin A. Croft[5] and André R. Wyss[6]

[1]*Department of Biological Sciences, St Mary's University, San Antonio, TX, USA*
[2]*Department of Vertebrate Paleontology, Division of Paleontology, American Museum of Natural History, New York, NY, USA*
[3]*Richard Gilder Graduate School, American Museum of Natural History, New York, NY, USA*
[4]*Key Laboratory of Vertebrate Evolution and Human Origin, Institute of Vertebrate Paleontology and Paleoanthropology, Beijing, China*
[5]*Department of Anatomy, Case Western University School of Medicine, Cleveland, OH, USA*
[6]*Department of Earth Science, University of California, Santa Barbara, CA, USA*

Abstract

The phylogenetic relationships of notoungulates, an extinct group of predominantly South American herbivores, remain poorly resolved with respect to both other placental mammals and among one another. Most previous phylogenetic analyses of notoungulates have not included characters of the internal cranium, not least because few such features, including the bony labyrinth, have been described for members of the group. Here we describe the inner ears of the notoungulates *Altitypotherium chucalensis* (Mesotheriidae), *Pachyrukhos moyani* (Hegetotheriidae) and *Cochilius* sp. (Interatheriidae) based on reconstructions of bony labyrinths obtained from computed tomography imagery. Comparisons of the bony labyrinths of these taxa with the basally diverging notoungulate *Notostylops murinus* (Notostylopidae), an isolated petrosal from Itaboraí, Brazil, referred to Notoungulata, and six therian outgroups, yielded an inner ear character matrix of 25 potentially phylogenetically informative characters, 14 of them novel to this study. Two equivocally optimized character states potentially support a pairing of Mesotheriidae and Hegetotheriidae, whereas four others may be diagnostic of Notoungulata. Three additional characters are potentially informative for diagnosing more inclusive clades: one for crown Placentalia; another for a clade containing *Kulbeckia*, *Zalambdalestes*, and Placentalia; and a third for Eutheria (crown Placentalia plus stem taxa). Several other characters are apomorphic for at least one notoungulate in our study and are of potential interest for broader taxonomic sampling within Notoungulata to clarify currently enigmatic interrelationships. Measures of the semicircular canals were used to infer agility (e.g. capable of quick movements vs. lethargic movements) of these taxa. Agility scores calculated from these data generally corroborate interpretations based on postcranial remains of these or closely related species. We provide estimates of the low-frequency hearing limits in notoungulates based on the ratio of radii of the apical and basal turns of the cochlea. These limits range from 15 Hz in *Notostylops* to 149 Hz in *Pachyrukhos*, values comparable to the Asian elephant (*Elephas maximus*) and the California sea lion (*Zalophus californianus*) when hearing in air, respectively.

Key words: cochlea; CT; Hegetotheriidae; Interatheriidae; Mesotheriidae; Notoungulata; petrosal; phylogenetic characters; South America.

Introduction

Notoungulata was a taxonomically, morphologically and ecologically diverse group of nearly exclusively South American mammals that thrived during much of the Cenozoic (Simpson, 1948, 1967, 1980; Patterson & Pascual, 1968). Notoungulates are characterized by a distinctive 'crochet' on the metaloph of the upper molars and an expansive epitympanic sinus in the squamosal (Patterson, 1934b, 1936; Cifelli, 1993).

The relationship of notoungulates to other placental mammals is debated (see Cifelli, 1993; Horovitz, 2004; Billet, 2010; Agnolin & Chimento, 2011; Billet & Martin, 2011; O'Leary et al. 2013), as are many of the higher-level

Correspondence
Thomas E. Macrini, Department of Biological Sciences, One Camino Santa Maria, St Mary's University, San Antonio, TX 78228, USA.
T: +210 431 4304; F: +210 431 4363; E: tmacrini@stmarytx.edu

Accepted for publication *12 August 2013*

relationships within the group. Previous analyses of notoungulate interrelationships have relied primarily on dental, external cranial and limited postcranial characters (e.g. Cifelli, 1993; Madden, 1997; Shockey, 1997; Cerdeño & Bond, 1998; Nasif et al. 2000; Croft et al. 2004; Flynn et al. 2005; Croft & Anaya, 2006; Hitz et al. 2006; Billet et al. 2009; Billet, 2010, 2011; Shockey et al. 2012). Features of the skull interior have been sampled sparsely in previous analyses of notoungulates. Indeed, such characters have received scant attention in phylogenetic studies of mammals generally, for the obvious reason that they are difficult to assess by traditional comparative anatomical techniques, particularly in fossils.

Portions of the internal anatomy of the notoungulate auditory region are well known, however (e.g. Patterson, 1932, 1934a, 1936; Simpson, 1936; Gabbert, 2004). These earlier studies focused primarily on the anatomy of the auditory bulla, epitympanic sinus, external anatomy of the petrosal, middle ear cavity and auditory ossicles. A few characters from these regions of the skull have been incorporated into recent phylogenetic analyses (e.g. Billet, 2010, 2011). A richer understanding of the notoungulate internal cranial osteology began to emerge with the application of high-resolution X-ray computed tomography (HRXCT; Macrini et al. 2010) and, by extending this approach, the present study contributes to a burgeoning body of new information about internal anatomical characteristics of the notoungulate skull. HRXCT also was applied recently to an isolated presumptive notoungulate petrosal from Itaboraí, Brazil (Billet & de Muizon, 2013).

The bony labyrinth comprises the cochlear canal, vestibule and semicircular canals (MacIntyre, 1972). These structures house the cochlear duct, saccule plus utricle and semicircular ducts, respectively. The cochlea functions primarily in hearing, whereas the other structures are associated with spatial orientation and balance. The semicircular ducts detect angular acceleration of the head, and aid in stabilizing vision during motion (summarized by Spoor, 2003; Spoor et al. 2007; Cox & Jeffery, 2010).

The radius of curvature of the semicircular canals, scaled for body mass, is correlated with agility in many extant mammals (e.g. Spoor et al. 2007; Cox & Jeffery, 2010), and thus can be used to infer agility capabilities in extinct mammals (e.g. Silcox et al. 2009). Moreover, the bony labyrinth has proven to include phylogenetically informative character data in some groups of mammals (e.g. diprotodontian marsupials, Schmelzle et al. 2007; strepsirrhine primates, Lebrun et al. 2010).

The aim of the present paper is fourfold. First, we use HRXCT to image and digitally reconstruct the bony labyrinths of representatives of three notoungulate clades, an interathere (*Cochilius*), a hegetothere (*Pachyrukhos*) and a mesothere (*Altitypotherium*). We describe these digitally reconstructed inner ear endocasts and compare them with the previously described bony labyrinth of *Notostylops murinus*, a Paleogene notoungulate (Macrini et al. 2010), and a newly described isolated petrosal from Itaboraí, Brazil (cf. Notoungulata; Billet & de Muizon, 2013).

Second, we present a matrix of potentially phylogenetically informative inner ear characters scored across all sampled notoungulates in which they are known. Several characters in our matrix have not been described in the literature previously. We emphasize that this study represents a preliminary comparison of these characters among notoungulates and mammals in general; additional features and taxa are being examined in our ongoing studies.

Third, we compare various measures of the bony labyrinth of the notoungulates described here with those of selected extant mammals, to better understand the agility and potentially locomotor habits of these extinct species. Although *Altitypotherium* and *Cochilius* are known from sparse or not yet analyzed postcranial remains, other members of the clades to which they belong (Mesotheriidae and Interatheriidae, respectively) have well-characterized postcrania. Inner ears thus provide an independent source of data against which to test postcranially based hypotheses of locomotor agility.

Finally, we assess auditory capabilities of notoungulates based on dimensions of the cochlear canal from inner ear virtual endocasts. The ratio of the radii of the apical and basal turns of the cochlea is examined with respect to low-frequency (LF) hearing limits, following the methodology of Manoussaki et al. (2008). Extant mammals with LF hearing below the human limit (i.e. mammals capable of detecting infrasound) utilize interaural time differences to localize sound (Manoussaki et al. 2008; Grothe et al. 2010). In some cases this capability is associated with LF communication (e.g. elephants) and long-distance hearing, particularly in species living in open habitats (e.g. some desert rodents), perhaps potentially related to predator avoidance (Grothe et al. 2010).

Materials and methods

Institutional abbreviations

FMNH, The Field Museum, Chicago, IL, USA; MNHN-F-BRD, Brazil fossil collections, Muséum national d'Histoire naturelle, Paris, France; SGOPV, vertebrate paleontology collections, Museo Nacional de Historia Natural, Santiago, Chile.

Specimens

Skulls of each of three groups of typothere notoungulates (Interatheriidae, Hegetotheriidae, Mesotheriidae) were analyzed using HRXCT. The resulting images and virtual reconstructions deriving therefrom were compared with the inner ear of *Notostylops* (Notostylopidae), recently documented through similar means (Macrini et al. 2010). Comparisons are also made to MNHN-F-BRD 23, a recently described isolated petrosal tentatively referred to the Notoungulata by Billet & de Muizon (2013). Specimens examined are listed in Table 1.

Table 1 Scan parameters for notoungulates examined in this study.

Species	Clade	Specimen #	Z (mm)	X, Y (mm)	# of slices
Altitypotherium chucalensis	Mesotheriidae	SGOPV 4100	0.0512	0.044	799
Cochilius sp.	Interatheriidae	SGOPV 3774	0.0690	0.060	1066
Notostylops murinus	Notostylopidae	FMNH P13319	0.0684	0.062	1599
Pachyrukhos moyani	Hegetotheriidae	FMNH P13051	0.0386	0.030	1200

X, Y, reconstructed pixel sizes in the X and Y planes; Z, interslice spacing.

The skull of *Altitypotherium chucalensis* investigated here (SGOPV 4100) was originally described and illustrated by Croft et al. (2004, fig. 9). This specimen is part of the Chucal Fauna, a high-altitude site on the Altiplano of northern Chile. The fauna, ~18 Ma (late early Miocene) in age, pertains to the Santacrucian South American Land Mammal 'Age' (SALMA; Croft et al. 2004).

The skull of *Cochilius* sp. (SGOPV 3774) analyzed here is from a fauna discovered near the Upeo River in east central Chile. This fauna is one of more than a dozen uncovered in volcaniclastic horizons of the Abanico Formation of the Andean Main Range in recent years (Flynn et al. 2012). The enormously thick (2–3 km) and geographically widespread Abanico Formation and its lateral equivalents have proven challenging to date radioisotopically, but currently appear to span much of Paleogene and early Neogene time. In the Upeo region fossiliferous horizons likely pertain to the Deseadan SALMA, although the fauna has yet to be fully analyzed, and thus SGOPV 3774 is approximately 29–24 Ma in age (Flynn et al. 2012).

The skull of *Pachyrukhos moyani* (FMNH P13051) examined here, representing a juvenile individual, was collected from Killik Aike Norte (Felton's Estancia), Río Gallegos, Santa Cruz Province, Argentina. Marshall (1976) provided a useful overview of this and other Santa Cruz Formation localities, of which Vizcaíno et al. (2012) provided a recent update. Patterson (1936) briefly described the bulla, middle ear and other aspects of the auditory anatomy of a different specimen of *P. moyani*, but the inner ear was not accessible to him.

CT scanning and digital endocast reconstruction

The three skulls were scanned in their entirety in the coronal plane at the Center for Quantitative X-ray Imaging at Pennsylvania State University (www.cqi.psu.edu) in University Park, PA, USA. Scan data were reconstructed as 1024×1024 pixel, 16-bit TIFF slices (i.e. images). Scanning parameters (e.g. slice thicknesses, pixel dimensions) are given in Table 1. Digital endocasts were extracted using the segmentation tools of Avizo 5.0 (2008, Visualization Sciences Group, www.vsg3d.com) and VGStudio 1.2 (2004, Volume Graphics GmbH, www.volumegraphics.com) following the protocols of Macrini et al. (2010) and Ni et al. (2012), respectively.

Reference is made to specific CT slices in the descriptions that follow. The prefix 'C' designates an image from the coronal plane (transverse plane of some authors), for example, C0800 is the 800th coronal slice, with slices being numbered from anterior to posterior.

Measurements

The inner ear dimensions described by Spoor & Zonneveld (1995) were taken from the reconstructed three-dimensional (3-D) digital models using the '3-D measure tool' of Avizo following the protocol described by Macrini et al. (2010). The measurement technique employed here differs slightly from that of Spoor et al. (2007), but there is no effect on calculated agility scores. The axes measured are illustrated in Fig. 1. Linear dimensions reported here (Table 2) are the mean of three replicate measurements. Following Spoor & Zonneveld (1998), we calculated radius of curvature (R) of each canal using the equation: $R = ([H + W]/4)$ where H = height [dorsoventral dimension of the anterior semicircular canal (ASC) and posterior semicircular canal (PSC); anteroposterior dimension or length (L) of the lateral semicircular canal (LSC)] and W = width of canal. Volumes of the digitally reconstructed endocasts were calculated in Avizo (Table 2).

Inferring locomotor agility

Locomotor agility scores for notoungulates were inferred using equations (Silcox et al. 2009; Table 3) derived from comparisons of semicircular canal radii of curvature, body masses and agility scores of 210 extant mammals from the work of Spoor et al. (2007). Spoor et al. (2007) scored the agility of modern taxa on a scale of 1 (sluggish) to 6 (agile/quick moving) based on field observations and data from the literature.

Body masses were taken from the literature and/or estimated from preserved cranial remains using published regressions for extant mammals (Tables 2 and 4). In all cases, body masses were estimated using the specimens from which semicircular canal dimensions were measured. Ranges of locomotor agility scores were calculated to reflect a range of body mass estimates in the literature (Table 5). Locomotor agility inferences are reported in Table 5.

Estimating auditory capabilities

The ratio of the radii of the innermost (apical) and outermost (basal) turns of the cochlea is correlated with the limits of LF hearing based on a study of extant marine and terrestrial mammals (Manoussaki et al. 2008). The relationship between the limit of LF hearing and the ratio of cochlear radii is described by the equation: $f = 1507 \exp[-0.578\ (p - 1)]$, where f = LF hearing limit; p = radii ratio = R_{base}/R_{apex}; R_{apex} = radius of curvature of apex of cochlea; R_{base} = radius of curvature of base of cochlea (Manoussaki et al. 2008). R_{apex} and R_{base} were determined using the method of Manoussaki et al. (2008, fig. 4). Following the approach of Orliac et al. (2012b), we applied the above methodology to extinct taxa.

Character-taxon matrix

We scored 25 morphological characters of the inner ear across several taxa (Tables 6 and 7), including the three notoungulates described here (*Altitypotherium chucalensis, Cochilius* sp., *Pachyrukhos moyani*),

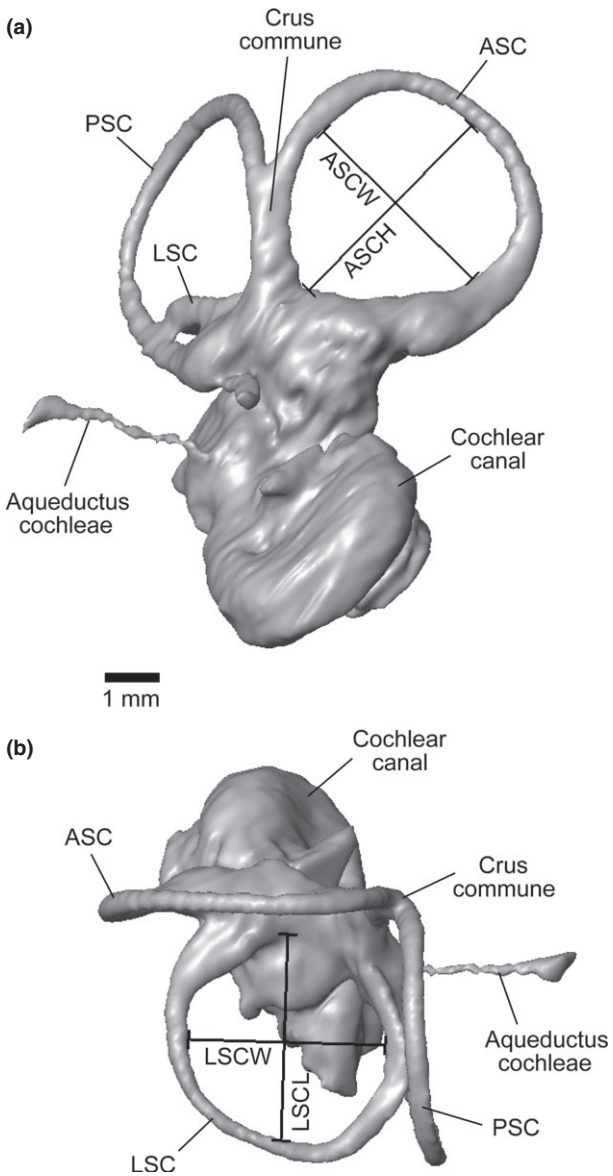

Fig. 1 Linear semicircular canal measurements taken on 3-D models of the inner ears obtained from CT imagery, as exemplified by the left inner ear model of *Notostylops murinus* (FMNH P13319); modified from Macrini et al. (2010, fig. 2). (a) Measurements of anterior semicircular canal shown in medial view; (b) measurements of lateral semicircular canal shown in dorsal view. Abbreviations: ASC, anterior semicircular canal; ASCH, anterior semicircular canal height; ASCW, anterior semicircular canal width; LSC, lateral semicircular canal; LSCL, lateral semicircular canal length; LSCW, lateral semicircular canal width; PSC, posterior semicircular canal.

Notostylops murinus (from Macrini et al. 2010), MNHN-F-BRD 23 (cf. Notoungulata) based on Billet & de Muizon (2013), and several therian outgroups. Outgroups included the extinct primate *Chilecebus carrascoensis* (from Ni et al. 2010); *Caluromys philander*, the woolly opossum (from Sánchez-Villagra & Schmelzle, 2007); the 'condylarth' *Hyopsodus lepidus* (AMNH 143783, from Orliac et al. 2012a; Benoit et al. 2013); and the stem placentals *Ukhaatherium gobiensis*, *Kulbeckia kulbecke* and *Zalambdalestes lecheyi* (from Wible et al. 2004, 2007; Ekdale & Rowe, 2011). We used several outgroups because many of the characters are new, making their polarities and the taxonomic level of their phylogenetic significance uncertain.

We examined the distributions of these character states on a pruned consensus topology of notoungulate relationships following the analyses of Cifelli (1993), Billet (2011) and Shockey et al. (2012). Relationships of the outgroups sampled in our analysis follow the topology of Wible et al. (2007). One exception is the use of *Chilecebus*, an extinct primate with a published CT analysis of its inner ear (Ni et al. 2010), which was substituted as an exemplar primate for the more inclusive clade 'Primates' analyzed by Wible et al. (2007) because the ancestral condition for inner ear characters is unknown for the entire primate clade. Character states were examined using the parsimony ancestral character state reconstruction option in Mesquite (version 2.74; Maddison & Maddison, 2010), which utilizes DELTRAN, delayed transformations, for missing character states.

Description

Below we describe 3-D reconstructions of the inner ears of three notoungulates, comparing them with *Notostylops murinus* (Macrini et al. 2010), MNHN-F-BRD 23 (cf. Notoungulata) based on Billet & de Muizon (2013), and various other therians, fossil and extant. These comparisons yielded the matrix of inner ear characters provided in Tables 6 and 7.

Altitypotherium chucalensis (Mesotheriidae)

Cochlear canal

We extracted a digital endocast of the bony labyrinth of *Altitypotherium* from the left petrosal, the more complete of the two petrosals. The great length of the cochlear canal relative to the size of the entire endocast is the most noteworthy feature of the inner ear of *Altitypotherium* (Fig. 2). Despite its length, the cochlear canal occupies only about 64% of the total bony labyrinth volume (Table 2), comparable to *Notostylops* (66%; Macrini et al. 2010). The cochlea has 2.0 turns vs. the 2.25 turns of *Notostylops* (Table 8) and 2.75 turns in MNHN-F-BRD 23 (Billet & de Muizon, 2013).

The primary and secondary osseous spiral laminae are visible in the cochlear canal, as in *Notostylops* (Macrini et al. 2010) and therians generally (Meng & Fox, 1995; Luo et al. 2011). The primary osseous spiral lamina projects from the meatal (inner) wall of the cochlear canal (e.g. C0342), whereas the secondary osseous spiral lamina projects from the radial (outer) wall (e.g. C0398). These structures leave troughs on the external surface of the cochlear canal portion of the inner ear endocast. The secondary osseous lamina extends through the first half of the basal turn of the cochlea, as in *Notostylops* (Macrini et al. 2010).

The canal housing the spiral ganglion of the cochlear nerve is visible within the first turn of the primary osseous spiral lamina (C0321-0338; Fig. 3). Cells of this ganglion synapse with cochlear hair cells (Gray, 1977; Luo & Marsh, 1996). The tractus spiralis foraminosus, which connects the

Table 2 Measurements of notoungulate bony labyrinths.

Species	*Altitypotherium chucalensis*	*Pachyrukhos moyani*	*Notostylops murinus*	*Cochilius* sp.
Specimen number	SGOPV 4100	FMNH P13051	FMNH P13319	SGOPV 3774
Body mass estimate (g)	8900–12800[3]	275–551[3]	3119[4]	1200–2400[3]
Skull length	160.0 mm[5]	44.1 mm	99.6 mm	72.4 mm
Petrosal sampled	Left	Right	Left	Right
Cochlea volume[1]	122.4 mm^3	17.8 mm^3	28.0 mm^3	21.7 mm^3
Vestibule volume	37.4 mm^3	4.5 mm^3	8.8 mm^3	14.0 mm^3
SC volume[2]	31.7 mm^3	3.3 mm^3	5.4 mm^3	5.2 mm^3
Stapedial ratio	2.0	Damaged	1.6	Damaged
ASC height	5.03 mm	3.39 mm	4.28 mm	3.80 mm
ASC width	4.91 mm	3.85 mm	3.91 mm	3.27 mm
ASCR	2.49 mm	1.81 mm	2.05 mm	1.77 mm
LSC length	4.30 mm	2.97 mm	3.69 mm	2.93 mm
LSC width	4.80 mm	2.76 mm	3.51 mm	3.05 mm
LSCR	2.28 mm	1.43 mm	1.80 mm	1.50 mm
PSC height	4.66 mm	3.06 mm	4.00 mm	3.56 mm
PSC width	5.70 mm	3.36 mm	4.02 mm	4.35 mm
PSCR	2.59 mm	1.61 mm	2.01 mm	1.98 mm
SCR	2.45 mm	1.62 mm	1.95 mm	1.75 mm

Skull length measured from the anterior tip of the premaxillae to the end of the occipital condyles in Avizo based on the CT slices. Stapedial ratio approximated from the outline of the fenestra vestibuli. Number of cochlear turns determined using the method of West (1985). Radius of curvature (*R*) of semicircular canals calculated following Spoor & Zonneveld (1998). Measurements from *Notostylops murinus* originally reported by Macrini et al. (2010) included for comparative purposes.

[1]Includes aqueductus cochleae.

[2]Includes crus commune and ampullae.

[3]See Table 4 for explanation.

[4]From Croft (2000).

[5]Skull length estimated from the preserved part of the skull (Croft et al. 2004, fig. 9), and scaled to the full skull length of '*Plesiotypotherium*' *minus* of Cerdas, which has similar skull proportions (Townsend & Croft, 2010).

ASC, anterior semicircular canal; LSC, lateral semicircular canal; PSC, posterior semicircular canal; *R*, radius of curvature; SC, semicircular canal; SCR, average semicircular canal radius of curvature.

Table 3 Locomotor agility equations derived by Silcox et al. (2009) based on the dataset of Spoor et al. (2007).

Canal	Equation
ASCR	$\log_{10}AGIL = 0.850–0.153(\log_{10}BM) + 0.706(\log_{10}ASCR)$
PSCR	$\log_{10}AGIL = 0.881–0.151(\log_{10}BM) + 0.677(\log_{10}PSCR)$
LSCR	$\log_{10}AGIL = 0.959–0.1670(\log_{10}BM) + 0.854(\log_{10}LSCR)$
SCR	$\log_{10}AGIL = 0.948–0.188(\log_{10}BM) + 0.962(\log_{10}SCR)$

AGIL, agility; ASCR, anterior semicircular canal radius of curvature; BM, body mass in grams; LSCR, lateral semicircular canal radius of curvature; PSCR, posterior semicircular canal radius of curvature; SCR, average semicircular canal radius of curvature.

spiral ganglion canal to cranial nerve VIII within the internal auditory meatus (Gray, 1977; Luo et al. 2011), is visible on the CT images of *Altitypotherium* (Fig. 3d).

The fenestra vestibuli (fenestra ovalis) lies diagonal to the plane of the LSC in an anteroventral to posterodorsal orientation (Fig. 2a), as in *Notostylops* (Macrini et al. 2010). The stapedial ratio (2.0), approximated from the outline of the fenestra vestibuli because the stapes itself is missing, contrasts with the ratios of 1.6 in *Notostylops* (Table 2) and 1.7 in the Itaboraí petrosal (Billet & de Muizon, 2013).

Although the fenestra cochleae (fenestra rotunda) could only be partially reconstructed due to damage, it appears to face posterolaterally (Fig. 2a), as in *Notostylops* (Macrini et al. 2010). Damage to the medial portion of the petrosal precludes a clear reconstruction of the aqueductus cochleae (cochlear aqueduct) from the CT imagery.

Vestibule

The recessus sphericus, which housed the saccule (sacculus), is significantly smaller and less rounded (Fig. 2c) than in *Notostylops* (Macrini et al. 2010). The utricular cavity is larger than the recessus sphericus (Fig. 2d). Nevertheless, the utricule is much smaller relative to the rest of the vestibule, and more posteriorly located, than in *Notostylops* (Macrini et al. 2010).

The canal leading from the posterior ampulla to the foramen singulare (Fig. 2b), an opening in the internal auditory meatus, is longer and thinner (relative to the thickness of the semicircular canals) than in *Notostylops* (Macrini et al. 2010). This canal probably transmitted the nervus ampullaris posterior, a branch of the vestibular nerve (Gray, 1977). The

Table 4 Explanation of how body mass estimates were determined for this study.

Taxon	Body mass range estimate	Explanation
Altitypotherium chucalensis	8.9–12.8 kg	Based on head-body length of 72–80 cm, which is estimated as 4.5–5× skull length based on reconstructions of *Trachytherus* and other typotheres. Skull length is estimated as 16 cm based on holotype of *A. chucalensis* and comparison with *'Plesiotypotherium' minus* of Cerdas (Townsend & Croft, 2010). Equations: Jerison, 1971 (light habitus); Silva & Downing, 1995 (all mammals, all rodents).
Cochilius sp.	1.2–2.4 kg	Based on head-body length of 36.5 cm, which is estimated at 5× skull length based on reconstructions of the interatheres *Protypotherium* and *Miocochilius*. Equations: Damuth, 1990 (non-selenodonts); Jerison, 1971 (light habitus); Silva & Downing, 1995 (all mammals).
Pachyrukhos moyani (adult)	0.9–1.8 kg	Mass is estimated at 0.8–1.1 kg based on an average head-body length of 33 cm (Sinclair, 1909: plate 11). Equations: Damuth, 1990 (non-selenodonts); Jerison, 1971 (light habitus); Silva & Downing, 1995 (all mammals). Mean craniodental estimates span 1.6–2.6 kg (Cassini et al. 2012a, appendix 1; Cassini et al. 2012b, table 14.3). Mean postcranial estimates span 0.9–5.0 kg, with a grand mean of preferred estimates of 1.8 kg (Elissamburu, 2012, table 2).
Pachyrukhos moyani (juvenile)	0.153–0.306 kg	Determined by geometrically scaling specimen FMNH P13051, a juvenile with skull length = 4.4 cm, with the adult average of 7.95 cm (Sinclair, 1909, plate 11). The geometric scaling was calculated as 17%, and this value was multiplied by body mass estimate range for the adult *Pachyrukhos* that is shown above.

Table 5 Inferred locomotor agility scores for selected notoungulates.

Species	*Altitypotherium chucalensis*	*Pachyrukhos moyani*	*Notostylops murinus*	*Cochilius* sp.
Specimen number	SGOPV 4100	FMNH P13051	FMNH P13319	SGOPV 3774
$AGIL_{ASCR}$	3.2–3.4	4.5–5.0	3.4	3.2–3.6
$AGIL_{PSCR}$	3.5–3.7	4.4–4.9	3.6	3.7–4.1
$AGIL_{LSCR}$	3.8–4.0	4.7–5.3	3.9	3.5–3.9
$AGIL_{SCR}$	3.5–3.8	4.8–5.5	3.7	3.5–4.0

Locomotor agility scale (ranging from 1 to 6, from poor to high agility) is based on qualitative field observations of extant mammals (Spoor et al. 2007). Scores are given as ranges for specimens having multiple body mass estimates.
$AGIL_{ASCR}$, $AGIL_{LSCR}$, $AGIL_{PSCR}$, $AGIL_{SCR}$, agility scores calculated from the anterior, lateral, posterior and average radius of curvature of the semicircular canals, respectively.

cross-sectional diameter of the aqueductus vestibuli (vestibular aqueduct), which housed the endolymphatic duct, is much greater in *Altitypotherium* (Fig. 2) than in *Notostylops* (Macrini et al. 2010).

Semicircular canals

The PSC has the largest radius of curvature of the three semicircular canals, followed closely by the ASC, and then more distantly by the LSC (Table 2). The PSC is the most elliptical in outline, whereas the ASC is the most circular (Table 2), the opposite of the condition in *Notostylops* (Macrini et al. 2010). The ASC is planar (Fig. 2d) unlike the other two canals, which undulate. The posterior arm of the LSC bends immediately outside the vestibule (Fig. 2b), and similarly the PSC deviates from a plane (Fig. 2d).

The crus commune is more robust compared with the thickness of the individual semicircular canals (Fig. 2) than in *Notostylops* (Macrini et al. 2010). The ASC and PSC of *Altitypotherium* extend little beyond the dorsal margin of the crus commune, unlike in *Notostylops* where they project considerably farther (Macrini et al. 2010). The crus commune extends 73% of the height of the ASC, whereas in *Notostylops* the crus extends only 64% of this height.

The anterior and posterior ampullae (Fig. 2) are more pronounced than in *Notostylops* (Macrini et al. 2010), being significantly more inflated than the semicircular canals. The anterior and lateral ampullae attach to the vestibule in the same horizontal plane as the LSC; the posterior ampulla, however, is located posteroventral to the crus commune and the entry of the posterior arm of the LSC into the vestibule (Fig. 2a).

The LSC and PSC extend equally far laterally when viewed dorsally (Fig. 2d). No secondary crus commune occurs between these two canals unlike the condition in MNHN-F-BRD 23 (Billet & de Muizon, 2013).

Table 6 Inner ear characters.

1	Lateral reach of LSC and PSC: equivalent (0); LSC terminates more medially than PSC (1) (modified from Schmelzle et al. 2007, character #4). State 1.0 is illustrated for *Altitypotherium* (Fig. 2d), and state 1.1 is shown for *Cochilius* (Fig. 6d).
2	Form of LSC in its transition to the lateral ampulla: straight (0), or undulating (1) (Schmelzle et al. 2007, character #6). State 2.0 is illustrated for *Altitypotherium* (Fig. 2a), and state 2.1 is shown for *Cochilius* (Fig. 6a).
3	Form of LSC at its transition to vestibule: straight (0), or undulating (1) (Schmelzle et al. 2007, character #7). State 3.0 is shown for *Cochilius* (Fig. 6a), and state 3.1 is present in *Altitypotherium* (Fig. 2a).
4	Posterior arm of the LSC in relation to the level of the PSC: anterior or even with the level of the PSC (0), or extends posterior to the level of the PSC (1) (modified from Schmelzle et al. 2007, character #8). State 4.0 is illustrated for *Altitypotherium* (Fig. 2d), and state 4.1 is shown for *Pachyrukhos* (Fig. 4d).
5	Shape of the PSC when viewed in the plane of the canal: mostly in the same plane (0), or curved such that the superior and inferior arms are not aligned when PSC is viewed dorsally (1) (modified from Schmelzle et al. 2007, character #9). State 5.0 is illustrated for *Cochilius* (Fig. 6d) and state 5.1 is shown for *Altitypotherium* (Fig. 2d).
6	Semicircular canal with largest overall radius of curvature: ASC (0), or PSC (1). New character. See Table 2 for calculation of SSC radius of curvature. State 6.0 is present in *Pachyrukhos* (Table 2) and state 6.1 in *Altitypotherium* (Table 2).
7	Roundest semicircular canal: LSC (0), PSC (1) or ASC (2). New character. This is determined by comparison of length vs. width measurements of each SSC. State 7.0 occurs in *Pachyrukhos* (Table 2), state 7.1 in *Notostylops* (Macrini et al. 2010) and state 7.2 in *Altitypotherium* (Table 2).
8	Anterior and posterior ampullae dorsoventral girth relative to semicircular canal cross-sectional diameter: ampullae girth in the dorsoventral direction extend well beyond the SSC boundaries (0), or ampullae are not noticeably expanded anterodorsally beyond the plane of the SSC (1). New character. State 8.0 is present in *Pachyrukhos* (Fig. 4), and state 8.1 is illustrated for *Cochilius* (Fig. 6).
9	Anterior and lateral ampullae position: lie in the same or nearly the same horizontal plane as the LSC (0), or anterior ampulla is significantly dorsal to the lateral ampulla (1). New character. State 9.0 is illustrated for *Altitypotherium* (Fig. 2a), and state 9.1 is present in *Cochilius* (Fig. 6a).
10	Primary osseous spiral lamina: absent (0) or present (1) (Meng & Fox, 1995). This was scored directly from CT imagery, rather than from the inner ear endocasts. State 10.1 is present in *Notostylops* (Macrini et al. 2010, fig. 4). This character cannot be scored for *Cochilius* because of damage to the petrosal and poor contrast between bone and matrix in the CT slices.
11	Secondary osseous spiral lamina: absent (0) or present (1) (Meng & Fox, 1995). This was scored directly from CT imagery, rather than from the inner ear endocasts. State 11.1 is present in *Notostylops* (Macrini et al. 2010, fig. 4). This character cannot be scored for *Cochilius* due to damage to the petrosal and poor contrast between bone and matrix in the CT slices.
12	Length of secondary osseous lamina: extends well past the basal turn (0), or extends from fenestra cochleae only through the first half of the basal turn (1) (Luo & Eastman, 1995; Geisler & Luo, 1996; Luo & Marsh, 1996). State 12.1 is present in *Notostylops* (Macrini et al. 2010). This character cannot be evaluated for *Cochilius* owing to poor contrast between the bone and matrix.
13	Crus commune lumen diameter thickness relative to semicircular canals: crus diameter is significantly thicker than canals (0), or crus has a diameter similar to that of the canals (1). New character. State 13.0 is present in *Altitypotherium* (Fig. 2a), and state 13.1 is shown for *Pachyrukhos* (Fig. 4a).
14	Dorsal extent of ASC and PSC above the crus commune: only the ASC extends well dorsal to the crus (0), ASC and PSC both extend well dorsal to the crus commune (1) or neither canal extends well dorsal to the crus (2). New character. State 14.0 is illustrated for *Pachyrukhos* (Fig. 4a), state 14.1 is present in *Notostylops* (Macrini et al. 2010, fig. 3) and state 14.2 is shown for *Altitypotherium* (Fig. 2a).
15	Utricle and saccule housing: in a common chamber (0), or within distinct, separated chambers in bony labyrinth (1). New character. State 15.0 is illustrated for *Caluromys* (Sánchez-Villagra & Schmelzle, 2007, fig. 1), and state 15.1 is illustrated for *Pachyrukhos* (Fig. 4). Outside of notoungulates state 15.1 is also known in *Henkelotherium* (Ruf et al. 2009) and *Dryolestes* (Luo et al. 2011, 2012).
16	Position of chamber for utricle (in bony labyrinth) when viewed dorsally: bulge for the utricle positioned closer to the posterior end of the LSC than the anterior end (0), or centrally located between ends of the LSC (1). New character. We observed no instances of the utricular chamber being close to the anterior end of the LSC, and thus have not presented this possible condition as a separate character state. State 16.0 is illustrated for *Pachyrukhos* (Fig. 4d); state 16.1 is shown in *Cochilius* (Fig. 6d).
17	Thickness of canal connecting the posterior ampulla and foramen singulare (transmits nervus ampullaris posterior): less than that of semicircular canals (0), or equal to or exceeds that of semicircular canals (1). New character. State 17.0 is illustrated for *Altitypotherium* (Fig. 2b) with state 17.1 shown for *Pachyrukhos* (Fig. 4b). This structure is not seen in the 3-D model of *Caluromys* (Sánchez-Villagra & Schmelzle, 2007) and cannot be reconstructed in our specimen of *Cochilius* due to damage.
18	Posterior end of the canal for the aqueductus cochleae: extends posterior to the PSC (0), or does not extend posterior to the PSC (1). New character. State 18.0 is illustrated for *Notostylops* (Macrini et al. 2010, fig. 3), whereas state 18.1 is present in *Pachyrukhos* (Fig. 4). The aqueductus cochleae could not be reconstructed for *Altitypotherium* or *Cochilius* due to damage.

19 Thickness of aqueductus cochleae relative to that of the semicircular canals: similar (0), or aqueductus cochleae diameter less than that of semicircular canals (1). New character. State 19.0 is illustrated for *Caluromys* (Sánchez-Villagra & Schmelzle, 2007, fig. 1), and state 19.1 is present in *Notostylops* (Macrini et al. 2010, fig. 3). The aqueductus cochleae could not be reconstructed for *Altitypotherium* or *Cochilius* owing to poor preservation.

20 Stapedial ratio: rounded, < 1.8 (0); or elliptical, 1.8 or greater (1) (Rougier et al. 1998; character #127). State 20.0 is seen in *Notostylops* (Table 2) and most metatherians (Segall, 1970; Rougier et al. 1998; Horovitz et al. 2008), whereas state 20.1 is present in most eutherians including *Altitypotherium* (Table 2). The fenestra vestibuli of the specimens of *Pachyrukhos* and *Cochilius* examined are damaged, making their scoring uncertain.

21 Confluence between the inferior arm of the PSC and the posterior arm of the LSC near the mid-length of these semicircular canals: absent (0) or present (1). New character. State 21.0 is present in *Altitypotherium* (Fig. 2) and state 21.1 is seen in *Pachyrukhos* (Fig. 4).

22 Secondary crus commune: present (0) or absent (1). New character. State 22.0 is illustrated for *Caluromys* (Sánchez-Villagra & Schmelzle, 2007, fig. 1), and state 22.1 is present in all notoungulates described in this study (Figs 2, 4 and 6).

23 Fenestra cochleae position relative to fenestra vestibuli (in lateral view of the inner ear endocast): fenestra cochleae posterior to fenestra vestibuli (0) or fenestra cochleae posteromedial to fenestra vestibuli (1) (Wible et al. 2007, character #303). State 23.0 is illustrated for *Altitypotherium* (Fig. 2a), and state 23.1 is illustrated for *Ukhaatherium*, *Kulbeckia* and *Zalambdalestes* in Ekdale & Rowe (2011, fig. 6). This character cannot be scored for the specimen of *Cochilius* that we examined because of damage to the petrosal.

24 Fenestra cochleae orientation: fenestra opens posterolaterally (0) or fenestra faces posteriorly (1) (Bloch et al. 2007, character #106). State 24.0 is illustrated for *Altitypotherium* (Fig. 2). This character cannot be scored for *Cochilius* because of damage to the petrosal.

25 Diameter of fenestra cochleae relative to that of fenestra vestibuli: fenestra cochleae is larger (0) or fenestra vestibuli is larger (1). New character. We encountered no instances where these structures had the same diameter. State 25.0 is present in *Notostylops* (Macrini et al. 2010, fig. 3), and state 25.1 is illustrated by *Pachyrukhos* (Fig. 4). This character could not be scored for *Cochilius* and *Altitypotherium* due to incomplete preservation.

ASC, anterior semicircular canal; LSC, lateral semicircular canal; PSC, posterior semicircular canal; SSC, semicircular canals (collectively). Figures illustrating character states are listed.

Pachyrukhos moyani (Hegetotheriidae)

Cochlear canal

We reconstructed a digital endocast of the bony labyrinth of the better preserved right petrosal of *Pachyrukhos*. The cochlear canal, having ~2.0 turns as in *Altitypotherium*, occupies nearly 70% of the volume of the total bony labyrinth space (Tables 2 and 8). Primary and secondary osseous spiral laminae are visible in the CT slices; as in *Altitypotherium* they leave troughs on the exterior of the cast of the cochlear canal (Fig. 4). The secondary osseous lamina of *Pachyrukhos* (Fig. 4) extends through the first half of the basal turn of the cochlea as in *Altitypotherium* (Fig. 2) and *Notostylops* (Macrini et al. 2010). The canal for the spiral ganglion is visible inside the primary osseous spiral lamina through the first turn of the cochlea (C0330–0355; Fig. 5), as in *Altitypotherium*.

The fenestra vestibuli is damaged, making the stapedial ratio uncertain (Fig. 4a). The opening of the fenestra vestibuli in *Pachyrukhos* is oriented as in *Altitypotherium* (Fig. 2a), but is more dorsally positioned (Fig. 4a). The fenestra cochleae, which is largely intact, lies posterior and slightly ventral to the fenestra vestibuli (Fig. 4a); as in *Altitypotherium* and *Notostylops*, it opens posterolaterally. Despite incomplete preservation, the fenestra vestibule is clearly much larger than the fenestra cochleae (Fig. 4a), the opposite of the condition in *Notostylops* (Macrini et al. 2010).

The aqueductus cochleae projects posteromedially (Fig. 4), although less far posteriorly than in *Notostylops* (Macrini et al. 2010). This canal likely transmitted the perilymphatic duct, which communicated with the subarachnoid space of the endocranial cavity (Gray, 1977).

Vestibule

The recessus sphericus portion of the vestibule is large and rounded (Fig. 4c), as in *Notostylops* (Macrini et al. 2010). The space occupied by the utricle is much larger than in *Altitypotherium* (Fig. 2d); as in *Altitypotherium* it is more posteriorly positioned than in *Notostylops* (Macrini et al. 2010). The canal for the nervus ampullaris from the posterior ampulla to the foramen singulare is roughly as wide as the semicircular canals (Fig. 4b), unlike in *Altitypotherium* (Fig. 2b) and *Notostylops* (Macrini et al. 2010), in which the canal is thinner. The aqueductus vestibuli of FMNH P13051 is not resolved in our imagery.

Semicircular canals

The ASC is the largest semicircular canal, as in the Itaboraí petrosal (Billet & de Muizon, 2013), followed closely by the PSC and more distantly by the LSC (Table 2). The ASC is the most elliptical of the three, and the LSC is the roundest (Table 2). The LSC undulates in profile, with its ventralmost point being approximately halfway between its connections to the vestibule (Fig. 4a). The

Table 7 Taxon-inner ear character matrix.

Taxon	1	2	3	4	5	6	7	8	9	10	11	12	13	14	15	16	17	18	19	20	21	22	23	24	25
Caluromys	0	0	0	0	0	0	0	0	0	1	1	0	0	0	0	0	?	0	0	0	0	0	0	0	0
†*Ukhaatherium*	0	0	0	0	1	0	0	0	1	?	?	?	0	0	?	?	?	?	?	1	0	0	1	?	?
†*Kulbeckia*	0	0	0	0	1	0	1&2	0	0	1	1	0	1	0	?	?	?	?	?	0&1	0	0	1	?	?
†*Zalambdalestes*	0	0	0	0	1	0	1	0	0	1	1	1	1	0	?	?	?	?	?	1	0	0	1	0	?
†*Chilecebus*	0	0	1	0	0	0	0	0	0	?	?	?	1	0	1	1	?	0	1	?	0	1	?	?	?
†*Hyopsodus*	0	1	0	0	0	0	0	0	0	?	1	?	1	0	0	?	?	1	0	?	0	0	?	1	?
†MNHN-F-BRD 23	0	0	0	0	0	0	0	0	0	1	1	1	1	1	?	?	1	0	1	0	0	0	0	0	0
†*Notostylops*	0	0	0	0	0	0	1	1	0	1	1	1	1	1	1	1	0	0	1	0	1	1	0	0	0
†*Altitypotherium*	0	0	1	0	1	1	2	0	0	1	1	1	0	2	1	0	0	?	?	1	0	1	0	0	?
†*Pachyrukhos*	0	0	1	1	1	0	0	0	0	1	1	1	1	0	1	0	1	1	1	?	1	1	0	0	1
†*Cochilius*	1	1	0	0	0	1	0	1	1	?	?	?	1	0	1	1	?	?	?	?	0	1	?	?	?

?, unknown. Character data sources: *Caluromys* (Sánchez-Villagra & Schmelzle, 2007); *Chilecebus* (Ni et al. 2010); *Hyopsodus* (AMNH 143783, inner ear endocast courtesy of Maeva Orliac; Benoit et al. 2013; Orliac et al. 2012a); *Kulbeckia* (Wible et al. 2004, 2007; Ekdale & Rowe, 2011); MNHN-F-BRD 23 (Billet & de Muizon, 2013); *Notostylops* (Macrini et al. 2010); *Ukhaatherium* (Wible et al. 2007; Ekdale & Rowe, 2011); *Zalambdalestes* (Wible et al. 2004, 2007; Ekdale & Rowe, 2011).
†, extinct taxon.

Table 8 LF limits and morphometric data for the inner ear of selected notoungulates.

Species	*Altitypotherium chucalensis*	*Pachyrukhos moyani*	*Notostylops murinus*	*Cochilius* sp.
Specimen number	SGOPV 4100	FMNH P13051	FMNH P13319	SGOPV 3774
# cochlear turns	2.0	2.0	2.25	2.0
Radii ratio	5.8	5	9	6
60-dB LF limit (Hz)	92	149	15	84

Radii ratio = R_{base}/R_{apex} (measured following the methods of Manoussaki et al. 2008); 60-dB LF limit calculated using equation of Manoussaki et al. (2008).
LF, low-frequency hearing; R_{apex}, radius of apex of cochlear canal; R_{base}, radius of base of cochlear canal.

ASC and PSC are planar, but the PSC is somewhat bowed (when viewed dorsally) in the rostrocaudal direction (Fig. 4d).

The crus commune (Fig. 4b) and semicircular canals are similar in thickness, whereas in *Altitypotherium* the crus is thicker (Fig. 2b). The ASC of *Pachyrukhos* extends well dorsal of the crus commune but the PSC does not (Fig. 4b). The crus commune of *Pachyrukhos* extends 65% of the height of the ASC, resembling *Notostylops*.

The maximum diameter of the anterior and posterior ampullae in the dorsoventral axis (Fig. 4a) exceeds the diameter of the semicircular canals, as in *Altitypotherium* (Fig. 2a). The anterior and lateral ampullae occur in the same horizontal plane as the LSC (as in *Notostylops,* Macrini et al. 2010; and *Altitypotherium,* Fig. 2); by contrast, the posterior ampulla lies ventral to this plane and posterior to the crus commune (Fig. 4a).

The PSC and LSC extend equally far laterally (Fig. 4d), as in *Notostylops* (Macrini et al. 2010) and *Altitypotherium* (Fig. 2d). The posterior arm of the LSC and the inferior arm of the PSC are confluent in *Pachyrukhos* (seen on both sides of the skull; Fig. 4), resembling *Notostylops* (Macrini et al. 2010).

Cochilius sp. (Interatheriidae)

Cochlear canal

We analyzed the better preserved right petrosal of *Cochilius* sp. (SGOPV 3774); this recently collected specimen has not yet been identified to species, and indeed *Cochilius* as a whole requires taxonomic revision. The cochlear canal makes up ~53% of the volume of the bony labyrinth (Table 2) and consists of 2.0 turns (Table 8). Damage to the petrosals and poor density contrast between the fossil and matrix of this specimen prevent reliable reconstructions of the fenestra vestibuli, fenestra cochleae and aqueductus cochleae. Similarly, it cannot be established whether primary and osseous spiral laminae are present, nor can the spiral ganglion canal be discerned.

Vestibule

The recessus sphericus portion of the vestibule for the saccule and the chamber for the utricle are separated within the bony labyrinth (Fig. 6), as in all other notoungulates examined (Figs 2 and 4; Macrini et al. 2010). The recessus sphericus of *Cochilius* is small (Fig. 6c), as in *Altitypotherium* (Fig. 2c), but the chamber for the utricule is large (Fig. 6d)

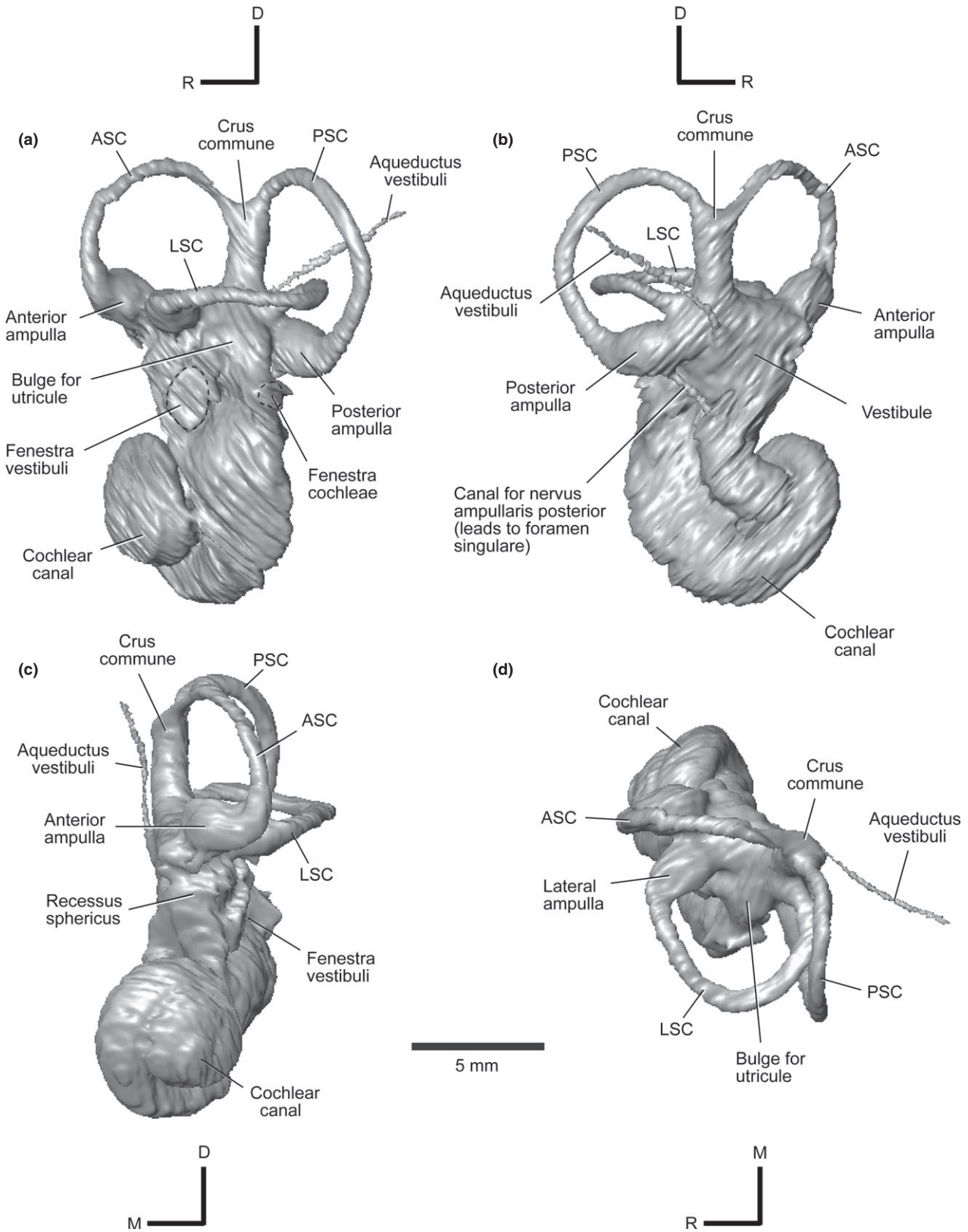

Fig. 2 Three-dimensional (3-D) reconstruction of the left inner ear of *Altitypotherium chucalensis* (SGOPV 4100) in (a) left lateral, (b) medial, (c) rostral and (d) dorsal views. Abbreviations: ASC, anterior semicircular canal; D, dorsal; LSC, lateral semicircular canal; M, medial; PSC, posterior semicircular canal; R, rostral. The fenestra vestibuli and fenestra cochleae are outlined with dashed lines. Scale bar is the same for all images (5 mm).

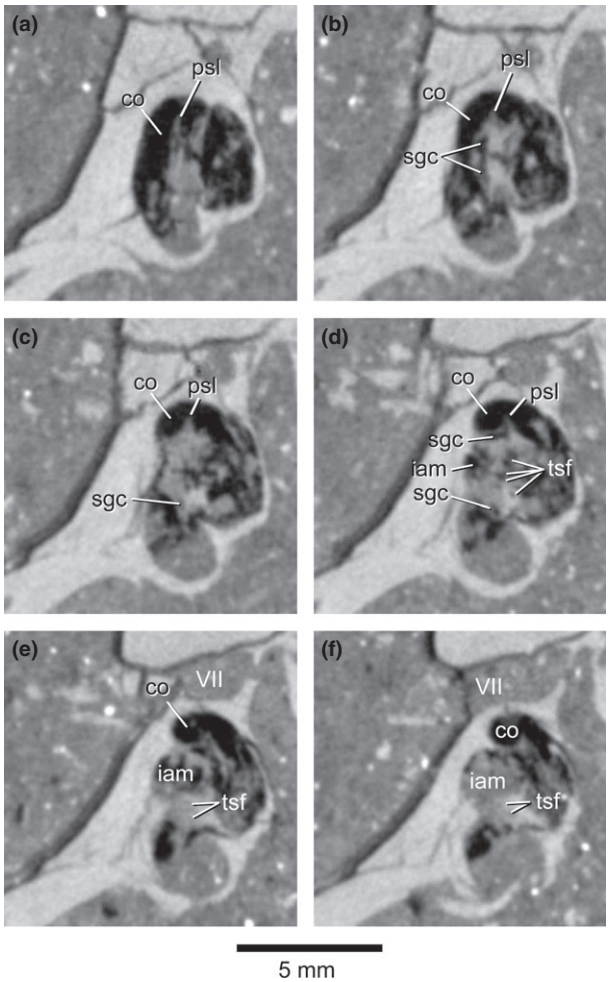

Fig. 3 Coronal CT images through the skull of *Altitypotherium chucalensis* (SGOPV 4100) cropped to show close-ups of the left petrosal. CT slices correspond to: (a) C0320; (b) C0325; (c) C0330; (d) C0335; (e) C0340; and (f) C0345; (a) being the most anterior image in the set. Abbreviations: co, cochlear canal; iam, internal auditory meatus; psl, primary osseous spiral lamina; sgc, spiral ganglion canal; tsf, tractus spiralis foraminosus; VII, marks space occupied by a branch of cranial nerve VII (facial nerve) during life. Note that the psl is the thin, white bony structure, and is surrounded by gray matrix. Scale bar is the same for all images (5 mm).

and centrally positioned relative to the ends of the LSC, as in *Notostylops* (Macrini et al. 2010). The canal from the posterior ampulla to the foramen singulare and the aqueductus vestibuli could not be reconstructed.

Semicircular canals

The PSC is the largest semicircular canal and the LSC the smallest (Table 2). The PSC is the most oval canal, and the LSC the roundest (Table 2). The LSC bends near the lateral ampulla (Fig. 6a), whereas the ASC and PSC are more planar, being slightly bowed in their respective planes when viewed dorsally (Fig. 6d), as is the PSC of *Pachyrukhos* (Fig. 4d).

The crus commune (Fig. 6b) and semicircular canals of *Cochilius* are comparable in thickness, as in *Pachyrukhos* (Fig. 4b) and *Notostylops* (Macrini et al. 2010), but not *Altitypotherium* (Fig. 2b). The ASC of *Cochilius* extends well dorsal to the crus commune but the PSC does not (Fig. 6b), both conditions as in *Pachyrukhos* (Fig. 4b). The crus commune of *Cochilius* extends 67% of the ASC height, similar to the conditions in *Pachyrukhos* and *Notostylops*.

The ampullae of *Cochilius* are similar in girth to their respective semicircular canals (Fig. 6), as in *Notostylops* (Macrini et al. 2010). The anterior ampulla is positioned anterior and slightly dorsal to the lateral ampulla, an unusual condition among notoungulates (Figs 2a and 4a; Macrini et al. 2010). The posterior ampulla is located significantly ventral to the other ampullae (Fig. 6a), as in other notoungulates.

The LSC extends less far laterally than the PSC (Fig. 6d), contrasting with the condition in other notoungulates (Figs 2d and 4d; Macrini et al. 2010). The LSC and PSC are not confluent at any point (Fig. 6), unlike in *Pachyrukhos* (Fig. 4d).

Discussion

Phylogenetically informative characters of the inner ear

Of the 25 inner ear characters considered here, 14 are new (Table 6). Ancestral character state reconstructions are presented in Table 9. Two characters (chars. 10 and 11) are invariant across our limited taxon sample (Fig. 7; Table 7), but may ultimately prove useful in broader samples. Another character state (char. 23.0) may represent a reversal or the ancestral condition for notoungulates, but could not be scored for *Cochilius* (Fig. 8). The remaining character states were apomorphic for at least one notoungulate in the matrix (Table 7). Of these, six are likely apomorphic for Notoungulata or clades within it, and one state is potentially synapomorphic for a more inclusive clade of eutherians.

Character state 3.1 (LSC undulating in its transition to the vestibule) and state 5.1 (PSC curved such that its superior and inferior arms are not aligned when viewed dorsally) are potentially apomorphic for *Altitypotherium* + *Pachyrukhos* (Table 7; i.e. Mesotheriidae and Hegetotheriidae). These character states also occur in various eutherian outgroups (Table 7), however, and in some diprotodontian marsupials (Schmelzle et al. 2007).

Character state 15.1 (utricle and saccule housed within distinct, separate chambers in bony labyrinth) is an equivocal synapomorphy for Notoungulata, as a distinct separation between these chambers in the bony labyrinth is not presently known in MNHM-F-BRD 23, and is absent in the nearest outgroup (*Hyopsodus*) but is present in the next most proximal outgroup, *Chilecebus* (Fig. 8).

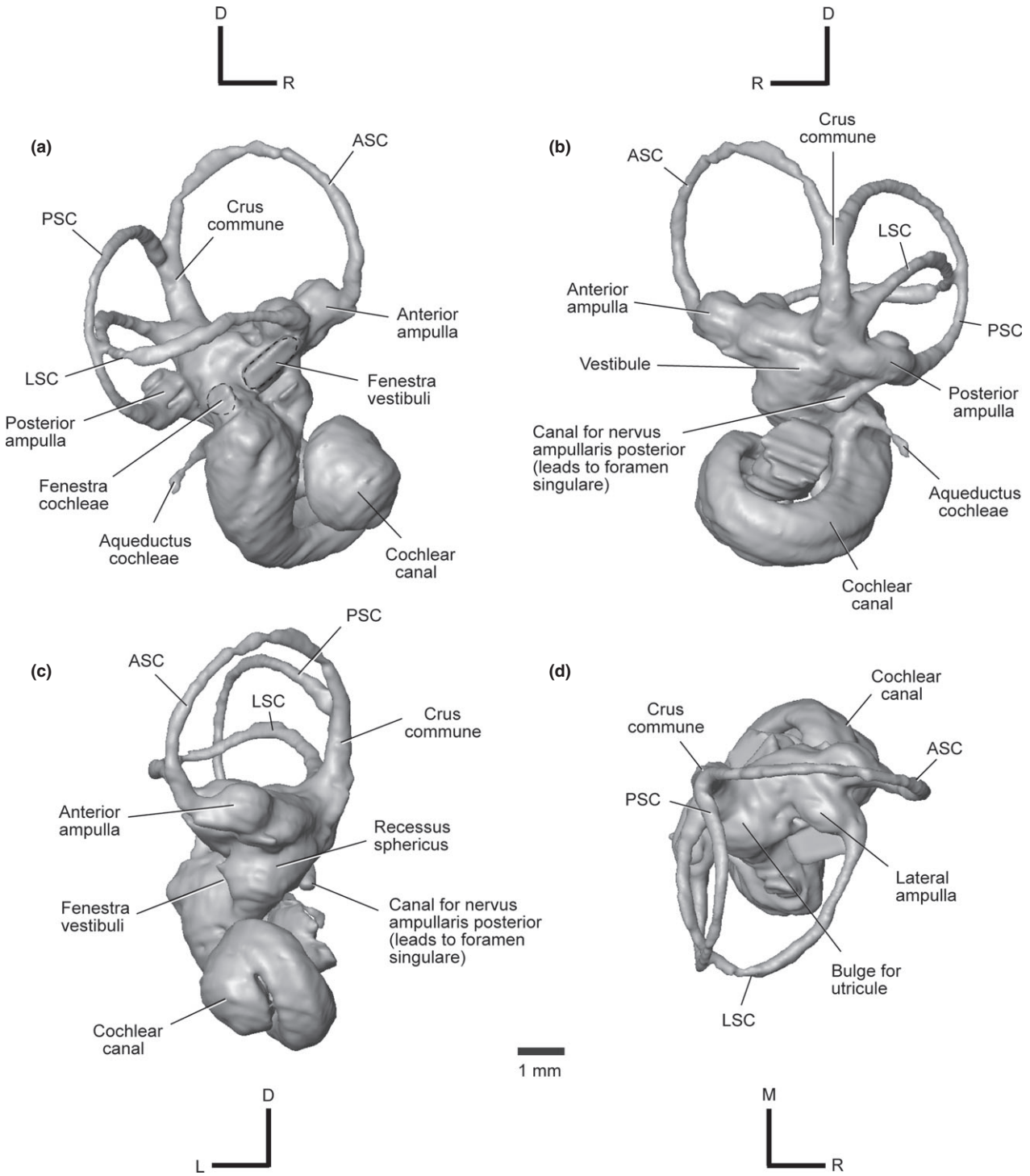

Fig. 4 Three-dimensional (3-D) reconstruction of the right inner ear of *Pachyrukhos moyani* (FMNH P13051) in (a) right lateral, (b) medial, (c) rostral and (d) dorsal views. Abbreviations: ASC, anterior semicircular canal; D, dorsal; L, lateral; LSC, lateral semicircular canal; M, medial; PSC, posterior semicircular canal; R, rostral. The fenestra vestibuli and fenestra cochleae are outlined with dashed lines. Scale bar is the same for all images (1 mm).

Character states 12.1 (secondary osseous lamina extends from fenestra cochleae through the first half of the basal turn) and 19.1 (aqueductus cochleae being much thinner than the semicircular canals) also are potential synapomorphies for Notoungulata, being shared by all sampled notoungulates preserving this region and absent in some outgroups (Fig. 8); these characters could not be evaluated in *Cochilius* due to incomplete preservation. In addition,

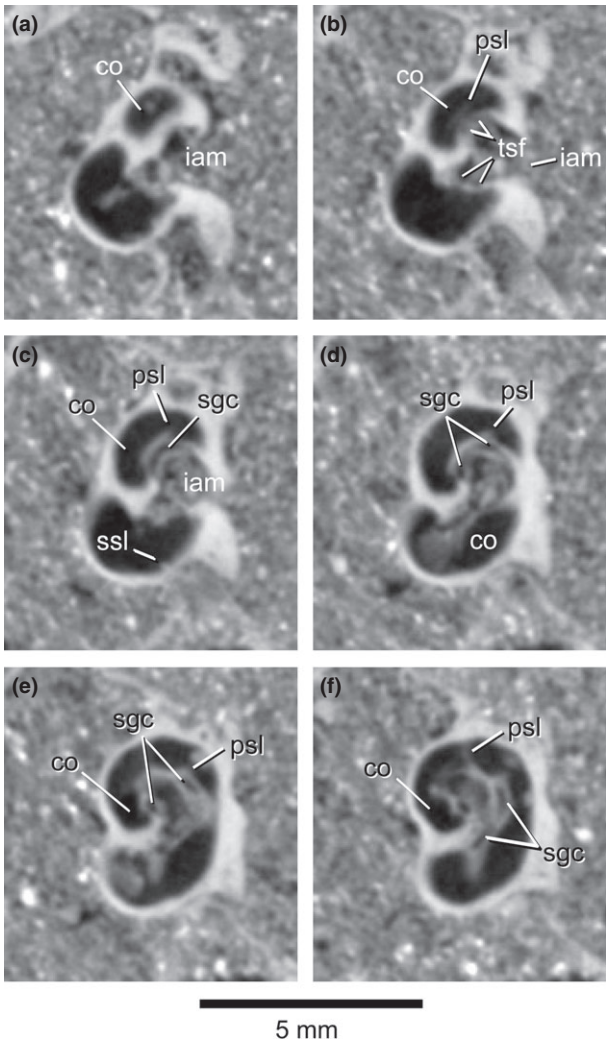

Fig. 5 Coronal CT images through the skull of *Pachyrukhos moyani* (FMNH P13051) cropped to show close-ups of the right petrosal. CT slices correspond to: (A) C0325; (B) C0330; (C) C0335; (D) C0340; (E) C0345; and (F) C0350; (A) being the most posterior image in the set. Abbreviations: co, cochlear canal; iam, internal auditory meatus; psl, primary osseous spiral lamina; sgc, spiral ganglion canal; ssl, secondary osseous spiral lamina; tsf, tractus spiralis foraminosus. Scale bar is the same for all images (5 mm).

these states occur variably among the outgroups in which they can be evaluated, further complicating resolution of their optimizations within Eutheria.

Character state 13.1 (diameter of crus commune lumen similar to that of the canals) is a potential synapomorphy for a clade of eutherians including *Kulbeckia*, *Zalambdalestes* and Placentalia (Fig. 8). Under this optimization, *Altitypotherium* is alone among Notoungulata and Placentalia in exhibiting a reversal to state 13.0 (crus commune lumen diameter is significantly greater than that of the semicircular canals).

Character state 16.1 (chamber for utricle when viewed dorsally is centrally located between ends of the LSC) is a potential synapomorphy for Placentalia, with a reversal (to state 16.0) in the clade containing *Pachyrukhos* and *Altitypotherium* (unnamed clade 4), with the caveat that the character condition is unknown in several outgroups (Fig. 8; Tables 7 and 9).

Character state 20.1 (stapedial ratio ≥ 1.8, i.e. elliptical) represents either an equivocal autapomorphy for *Altitypotherium*, or a synapomorphy for Eutheria with reversal in basal notoungulates, indicated by MNHM-F-BRD 23 and *Notostylops*, and a polymorphic condition for *Kulbeckia* (Table 7). The condition is unknown for *Cochilius*, *Pachyrukhos* and the outgroups *Hyopsodus* and *Chilecebus*, precluding a clear estimation of the ancestral condition for Placentalia.

Another character state of note, confluence of the LSC and PSC (state 21.1) near the mid-length of these semicircular canals (Fig. 4), occurs in *Notostylops* and *Pachyrukhos* (Table 7). Based on the phylogenetic hypothesis shown in Fig. 6, this condition appears to have evolved independently in these two taxa. Confluence of these canals is not reported for other mammals except in cases in which a secondary crus commune is formed (e.g. Hyrtl, 1845; Gray, 1907, 1908; Meng & Fox, 1995; Sánchez-Villagra & Schmelzle, 2007; Horovitz et al. 2008; Ladevèze et al. 2008), but the condition exhibited in these notoungulates is not a secondary crus. The presence of a secondary crus commune (state 22.0) is likely plesiomorphic for eutherians (Meng & Fox, 1995; Ekdale & Rowe, 2011), and possibly all therians (Ekdale, 2013), based on its presence in metatherians (Sánchez-Villagra & Schmelzle, 2007; Horovitz et al. 2008, 2009) and in dryolestoid mammals that are outgroups of crown Theria (Ruf et al. 2009; Luo et al. 2011, 2012). None of the notoungulates examined here possess a secondary crus, suggesting that a loss of this feature typifies Notoungulata (state 22.1; Fig. 8). Billet & de Muizon (2013) report a secondary crus commune in MNHN-F-BRD 23 (cf. Notoungulata), however.

The above results demonstrate that notoungulate inner ears hold phylogenetically significant information (Fig. 8), and that high-resolution CT analyses of endocranial anatomy have the potential to yield new characters for clarifying relationships that remain poorly resolved. Understanding the distribution of these characters and their utility in diagnosing various clades will benefit from broader sampling within Notoungulata and other mammals, thereby clarifying their phylogenetic relevance.

Comparison of AGIL (inner ear-based agility) scores with postcranial remains

Mesotheriidae

The limited postcranial material known for *Altitypotherium chucalensis* is currently undescribed (Croft et al. 2004). Mesotheres are considered scratch-diggers based on

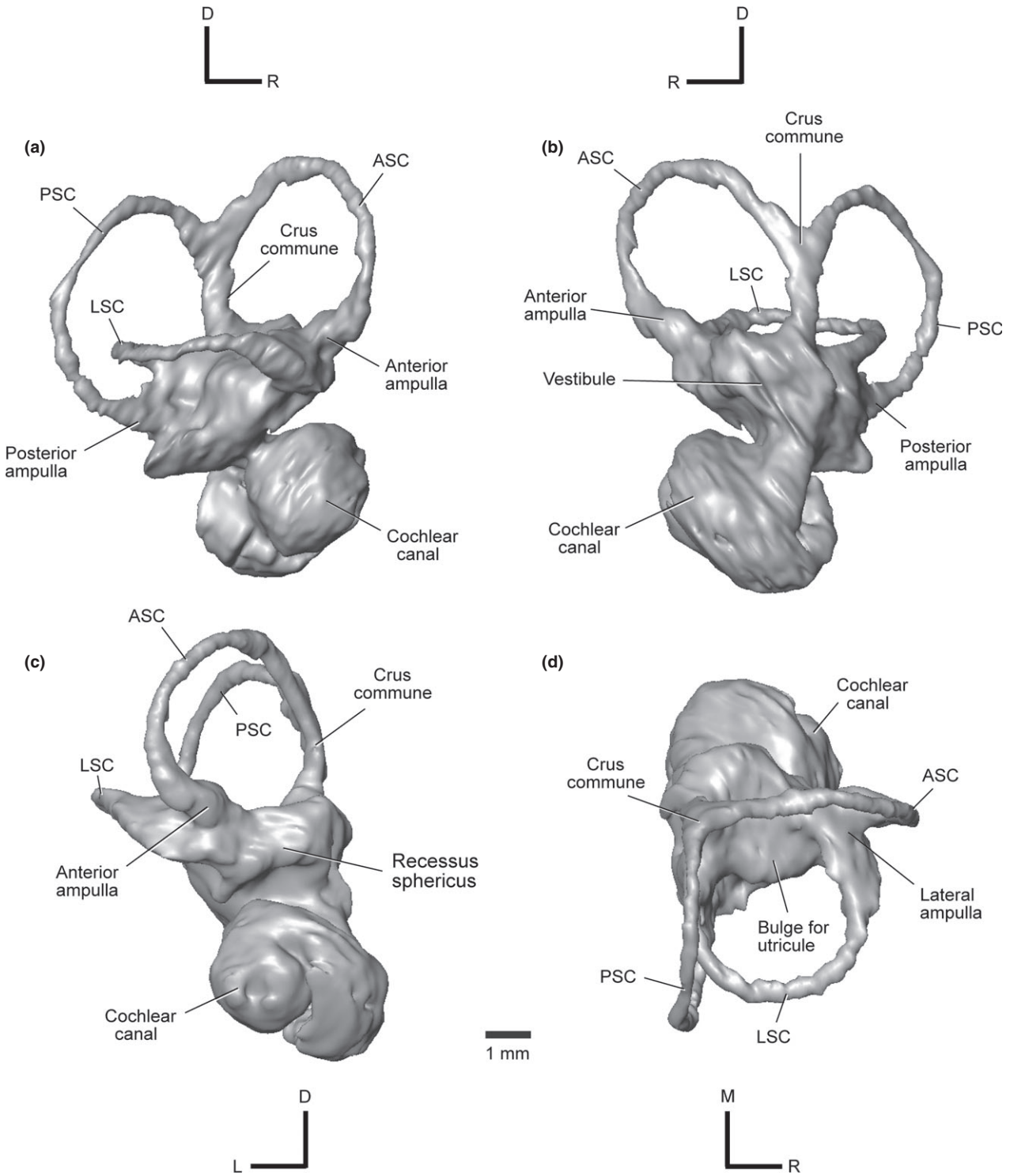

Fig. 6 Three-dimensional (3-D) reconstruction of the right inner ear of *Cochilius* sp. (SGOPV 3774) in (a) right lateral, (b) medial, (c) rostral and (d) dorsal views. Abbreviations: ASC, anterior semicircular canal; D, dorsal; L, lateral; LSC, lateral semicircular canal; M, medial; PSC, posterior semicircular canal; R, rostral. Scale bar is the same for all images (1 mm).

postcranial material of *Trachytherus*, *Plesiotypotherium* and *Mesotherium* (Shockey et al. 2007). Following the precepts of phylogenetic bracketing, it may be inferred that *Altitypotherium* is also a scratch-digger, inasmuch as it is nested within a clade including these other mesotheres with specialized habits.

Regressions of log-transformed semicircular canal dimensions and body masses, with log-transformed agility scores

Table 9 Parsimony ancestral state reconstructions.

Character	Theria[1]	Eutheria	Unnamed clade 1	Unnamed clade 2	Placentalia	Unnamed clade 3	Notoungulata	Typotheria	Unnamed clade 4
1	0	0	0	0	0	0	0	0	0
2	0	0	0	0	0	0	0	0	0
3	0	0	0	0	0	0	0	0	1
4	0	0	0	0	0	0	0	0	0
5	0/1	0/1	0/1	1	0	0	0	0	1
6	0	0	0	0	0	0	0	0/1	0/1
7	0	0	0	1	0	0	0	0	0
8	0	0	0	0	0	0	0	0	0
9	0	0	0	0	0	0	0	0	0
10	1	1	1	1	1	1	1	1	1
11	1	1	1	1	1	1	1	1	1
12	0/1	0/1	0/1	0/1	0/1	0/1	1	1	1
13	0	0	1	1	1	1	1	1	1
14	0	0	0	0	0	0	0/1	0	0
15	0/1	0/1	0/1	0/1	0/1	0/1	1	1	1
16	0/1	0/1	0/1	0/1	1	1	1	1	0
17	0/1	0/1	0/1	0/1	0/1	0/1	0/1	0/1	0/1
18	0	0	0	0	0	0	0	0/1	0/1
19	0/1	0/1	0/1	0/1	0/1	0/1	1	1	1
20	0/1	0/1	0/1	0/1	0/1	0/1	0/1	0/1	0/1
21	0	0	0	0	0	0	0	0	0
22	0	0	0	0	0/1	0/1	0/1	1	1
23	0/1	0/1	0/1	1	0/1	0/1	0	0	0
24	0	0	0	0	0	0	0	0	0
25	0	0	0	0	0	0	0	0/1	0/1

[1]Clade names correspond with those labeled in Fig. 7.

in living mammals (Table 3), indicate scores of 3.2–4.0 (average 3.6; Table 5) for *Altitypotherium*. These are somewhat higher than the 2–3 range ascribed to extant scratch-diggers (Spoor et al. 2007), indicating that *Altitypotherium* was a more generalized terrestrial mammal with fossorial tendencies, or that this scratch-digging notoungulate possessed a slightly different inner ear architecture than exemplars of extant mammals with similar specialization.

Interatheriidae

The postcranium of *Protypotherium* indicates that it was a generalized terrestrial mammal with cursorial tendencies (Croft & Anderson, 2008). Other interatheriids have been interpreted as more cursorial or as fossorial (summarized by Croft & Anderson, 2008; Shockey & Anaya, 2008; Cassini et al. 2012b).

The agility scores of *Cochilius* range from 3.2 to 4.1, averaging 3.7 (Table 5). Terrestrial artiodactyls and carnivorans sampled by Spoor et al. (2007) scored between 3 and 4, comparable to *Cochilius*. These scores, coupled with analyses of the postcrania of various interatheriids, seemingly suggest that *Cochilius* was a generalized terrestrial mammal with cursorial tendencies. However, its range of agility scores is also compatible with a wide variety of locomotor styles (generalized terrestrial, cursorial, scansorial, arboreal, semiaquatic or saltatorial) based on overlap with modern forms (Spoor et al. 2007). Our interpretation that *Cochilius* had generalized terrestrial locomotor capabilities with cursorial tendencies is provisional, requiring testing with postcranial data when they become available.

Hegetotheriidae

Pachyrukhos moyanoi may have been saltatory, judging from the length of its hind limbs and inner digits (Reguero et al. 2007; Cassini et al. 2012b), as well as from the presence of a long, slender, caudally projecting metacromion process of the scapula (Seckel & Janis, 2008). The postcranium of *Paedotherium* suggests cursorial and burrowing tendencies (Elissamburu, 2004), whereas the hind limb of *Prohegetotherium* is consistent with cursoriality (Shockey & Anaya, 2008).

Agility scores for *Pachyrukhos* range from 4.4 to 5.5 (average 4.9; Table 5). The upper end of this range approaches scores for extant saltatorial forms, which range from 5 to 6 in the Spoor et al. (2007) dataset. On the other hand, the lower end of this range and the average both point toward more generalized terrestrial locomotion with cursorial tendencies.

Locomotor patterns inferred from agility scores require testing with analyses of postcranial material given uncertainty inherent in AGIL calculations. Beyond variance about the means of the regressions on which AGIL values are

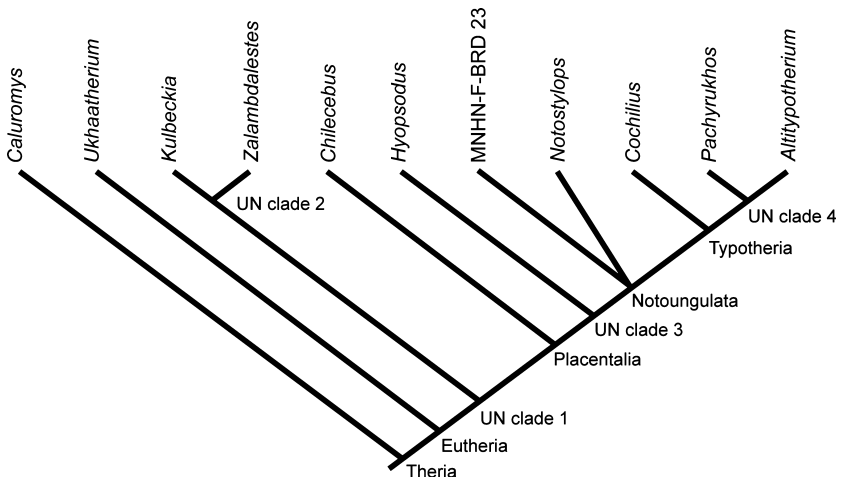

Fig. 7 Pruned consensus tree of the Notoungulata phylogenies published by Cifelli (1993, fig. 15.7), Billet (2011, fig. 9), Billet & de Muizon (2013, fig. 7) and Shockey et al. (2012, fig. 14), highlighting only those notoungulate taxa for which inner ear data are available. The genus names given presumably reflect the 'family' level relationships depicted in the cited studies: *Notostylops* (Notostylopidae); *Cochilius* (Interatheriidae); *Altitypotherium* (Mesotheriidae); and *Pachyrukhos* (Hegetotheriidae). Only further sampling will establish whether the conditions in the genera cited are indeed representative of the clades they represent. Outgroup relationships are based on the topology of Wible et al. (2007) for those taxa or members of the same clade (e.g. *Chilecebus* was substituted as a primate exemplar for the more inclusive terminal taxon 'Primates' used by Wible et al. 2007). Abbreviation: UN clade, unnamed clade.

based, sources of uncertainty include imprecision in estimating body mass for extinct taxa and the subjectivity of locomotor agility scores for extant mammals – given their basis in qualitative field observations (Spoor et al. 2007). These and other sources of error are considered more fully elsewhere (Macrini et al. 2010).

Auditory capabilities

Notoungulate LF hearing limits, as estimated from the equation of Manoussaki et al. (2008), are reported in Table 8. The LF hearing limits range from 15 Hz in *Notostylops* to 149 Hz in *Pachyrukhos*. The estimated LF hearing limit of *Notostylops* is comparable to that of *Elephas maximus*, the Asian elephant (17 Hz), and *Bos taurus*, the cow (23 Hz; based on the analysis of Manoussaki et al. 2008), whereas that of *Pachyrukhos* is most similar to *Tursiops truncatus*, the bottlenose dolphin (150 Hz in water), and *Zalophus californianus*, the California sea lion (180 Hz in air; Manoussaki et al. 2008). The LF hearing limit of *Altitypotherium* (92 Hz) is comparable to those of *Oryctolagus cuniculus*, the European rabbit (96 Hz), and *Saimiri sciureus*, the squirrel monkey (100 Hz; Manoussaki et al. 2008), whereas that for *Cochilius* (84 Hz; Table 8) lies between those of *Oryctolagus* and *Canis lupus familiaris*, the domestic dog (64 Hz; West, 1985).

Manoussaki et al. (2008) examined the relationship between LF hearing and cochlear metrics for both marine and terrestrial mammals, correcting for sound measurement differences in air vs. water. The small sample ($N = 13$) of their study included only taxa with 'generalist ears' (in their words; Manoussaki et al. 2008, pp. 6163–6164). Thus, the LF hearing estimates for notoungulates should be viewed in light of these limitations, and the significance of the ecological and habitat inferences drawn from these data should not be overstated. These results are open to any number of interpretations. For example, the extremely low LF hearing estimate in *Notostylops* might imply adaptations for hearing over long distances in open habitats, which is consistent with predator avoidance strategies in some extant desert rodents, or perhaps is associated with LF communication similar to that utilized by extant elephants and other large terrestrial mammals (Manoussaki et al. 2008; Grothe et al. 2010). Given the paucity of data on extant terrestrial taxa tuned to LF hearing, it is difficult to make more precise ecological and habitat inferences from the LF hearing estimates of the other extinct notoungulates in this study.

Conclusions

Anatomical descriptions of inner ears based on CT scans of three extinct, native South American ungulates presented above greatly augment our understanding of this region in notoungulates as a whole, and add to a growing library of anatomical data on the inner ears of mammals in general (e.g. Hyrtl, 1845; Gray, 1907, 1908; MacIntyre, 1972; Fleischer, 1973; Luo & Ketten, 1991; Meng & Fox, 1995; Sánchez-Villagra & Schmelzle, 2007; Schmelzle et al. 2007; Horovitz et al. 2008, 2009; Ladevèze et al. 2008; Ruf et al. 2009; Ekdale, 2010, 2011, 2013; Ni et al. 2010; Ekdale & Rowe, 2011; Luo et al. 2011; Billet & de Muizon, 2013).

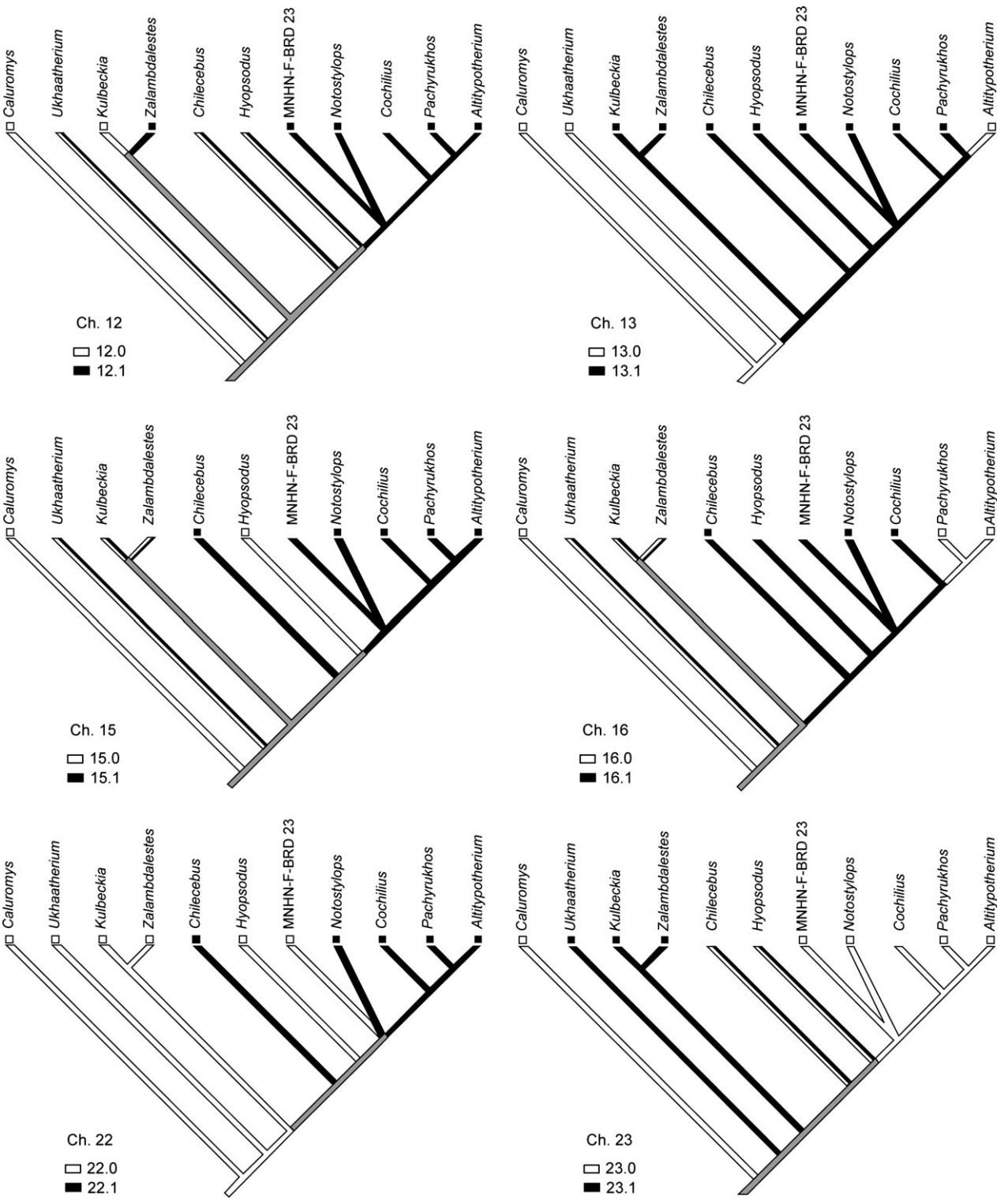

Fig. 8 Transformations of six characters based on DELTRAN optimization on the topology shown in Fig. 7. Gray fill represents ambiguous character reconstruction for a particular node. Striped branch leading to a terminal taxon indicates unknown character state for that particular taxon. Note: transformation for Character 15 is identical to that of a seventh character, Character 19 (not shown).

A central goal of this study was to extract phylogenetic information from the inner ears of notoungulates. To this end, we produced a character-taxon matrix consisting of 25 characters of the inner ear, 14 of them new, scored across a handful of notoungulates and multiple outgroups. Two character states support a pairing between Mesotheriidae

and Hegetotheriidae, and four are potential synapomorphies for Notoungulata. Three other characters represent potential synapomorphies for Placentalia, Eutheria and a clade of eutherians, including *Kulbeckia*, *Zalambdalestes*, plus Placentalia. Twelve other characters exhibited apomorphic states for one or more notoungulates. Although our taxonomic sampling in this initial analysis is limited, we will continue to broaden our sampling of taxa and endocranial characters, encouraging others to incorporate such features in phylogenetic analyses of notoungulates and other mammals. Only through such efforts will the potential phylogenetic significance of these characters be realized.

A second aim of this study, assessing the locomotor capabilities of these extinct taxa, was accomplished by deriving locomotor agility scores from morphometrics of the semicircular canals, following the methods of Silcox et al. (2009). Published analyses of the postcranial skeletons of these taxa, or close relatives, provide an important point of comparison to the agility scores deduced from the semicircular canal morphometrics. Agility scores and postcranial analyses yield generally consistent estimates of locomotor style. Minor discrepancies between results produced by the two methods may be ascribed to uncertainties in determining agility scores in living forms, or potentially to clade-specific distinctions among taxa with similar locomotor styles. Another issue is the fact that extant taxa with disparate locomotor styles sometimes exhibit broad overlap in agility scores.

Finally, we used data obtained from CT scan reconstructions to estimate auditory capabilities for the taxa surveyed. The radii of the apical and basal turns of the cochlea correlate with LF hearing limits (Manoussaki et al. 2008). On this basis, LF hearing limits for the sampled notoungulates ranged from 15 Hz in *Notostylops* to 149 Hz in *Pachyrukhos*, values comparable to the Asian elephant and cow for *Notostylops*, and the bottlenose dolphin and California sea lion for *Pachyrukhos*.

Acknowledgements

The authors thank Tim Ryan (Department of Anthropology; Center for Quantitative X-ray Imaging at Penn State University) for scanning the specimens. Maeva Orliac (Institut des sciences de l'évolution de Université Montpellier 2, France) graciously made images of a digital inner ear endocast of *Hyopsodus* (AMNH 143783) available for coding as an outgroup in our character matrix. We are grateful to The Field Museum and the Museo Nacional de Historia Natural (Santiago, Chile) for providing access to the notoungulate specimens scanned and analyzed for this study. Funding was provided by NSF DEB-0513476 to JJF and a Frick Postdoctoral Fellowship (2008–2009) from the Department of Vertebrate Paleontology at the AMNH to TEM. This work also represents a contribution to the AToL-Mammal Morphology studies supported by BIO EF- 0629811 (to JFF, XN and colleagues). We thank Zhe-Xi Luo and an anonymous reviewer for constructive comments that improved this paper. The authors have no conflicts of interest to declare.

References

Agnolin FL, Chimento NR (2011) Afrotherian affinities for endemic South American 'ungulates'. *Mamm Biol* **76**, 101–108.

Benoit J, Orliac M, Tabuce R (2013) The petrosal of *Chambius* (Macroscelidea, Afrotheria) from the Eocene of Djebel Chambi (Tunisia). *J Syst Palaeontol*, DOI: 10.1080/14772019.2012.713400.

Billet GB (2010) New observations on the skull of *Pyrotherium* (Pyrotheria, Mammalia) and new phylogenetic hypotheses on South American ungulates. *J Mamm Evol* **17**, 21–59.

Billet GB (2011) Phylogeny of the Notoungulata (Mammalia) based on cranial and dental characters. *J Syst Palaeontol* **9**, 481–497.

Billet G, de Muizon C (2013) External and internal anatomy of a petrosal from the Late Paleocene of Itaboraí, Brazil, referred to Notoungulata (Placentalia). *J Vertebr Paleontol* **33**, 455–469.

Billet G, Martin T (2011) No evidence for an afrotherian-like delayed dental eruption in South American notoungulates. *Naturwissenschaften* **98**, 509–517.

Billet G, Patterson B, de Muizon C (2009) Craniodental anatomy of late Oligocene archaeohyracids (Notoungulata, Mammalia) from Bolivia and Argentina and new phylogenetic hypotheses. *Zool J Linn Soc* **155**, 458–509.

Bloch JI, Silcox MT, Boyer DM, et al. (2007) New Paleocene skeletons and the relationship of plesiadapiforms to crown-clade primates. *Proc Natl Acad Sci USA* **104**, 1159–1164.

Cassini GH, Vizcaíno SF, Bargo MS (2012a) Body mass estimation in early Miocene native South American ungulates: a predictive equation based on 3D landmarks. *J Zool* **287**, 53–64.

Cassini GH, Cerdeño E, Villafañe AL, et al. (2012b) Paleobiology of Santacrucian native ungulates (Meridiungulata: Astrapotheria, Litopterna and Notoungulata). In: *Early Miocene Paleobiology in Patagonia: High-Latitude Paleocommunities of the Santa Cruz Formation*. (eds Vizcaíno SF, Kay RF, Bargo MS), pp. 243–286. New York: Cambridge University Press.

Cerdeño E, Bond M (1998) Taxonomic revision and phylogeny of *Paedotherium* and *Tremacyllus* (Pachyrukhinae, Hegetotheriidae, Notoungulata) from the late Miocene to Pleistocene of Argentina. *J Vertebr Paleontol* **18**, 799–811.

Cifelli RL (1993) The phylogeny of the native South American ungulates. In: *Phylogeny Mammal Volume 2: Placentals*. (eds Szalay FS, Novacek MJ, McKenna MC), pp. 195–216. New York: Springer.

Cox PG, Jeffery N (2010) Semicircular canals and agility: the influence of size and shape measures. *J Anat* **216**, 37–47.

Croft DA (2000) *Archaeohyracidae (Mammalia: Notoungulata) from the Tinguiririca Fauna, Central Chile, and the Evolution and Paleoecology of South American Mammalian Herbivores*. Chicago, IL: PhD dissertation,University of Chicago.

Croft DA, Anaya F (2006) A new middle Miocene hegetotheriid (Notoungulata: Typotheria) and a phylogeny of the Hegetotheriidae. *J Vertebr Paleontol* **26**, 387–399.

Croft DA, Anderson LC (2008) Locomotion in the extinct notoungulate *Protypotherium*. *Palaeontol Electron* **11**, 1–20.

Croft DA, Flynn JJ, Wyss AR (2004) Notoungulata and Litopterna of the early Miocene Chucal Fauna, northern Chile. *Fieldiana: Geol, New Series* **50**, 1–52.

Damuth J (1990) Problems in estimating body masses of archaic ungulates using dental measurements. In: *Body Size in Mammalian Paleobiology: Estimation and Biological Implications*

(eds Damuth J, MacFadden BJ), pp. 229–253. Cambridge: Cambridge University Press.

Ekdale EG (2010) Ontogenetic variation in the bony labyrinth of *Monodelphis domestica* (Mammalia: Marsupialia) following ossification of the inner ear cavities. *Anat Rec* **293**, 1896–1912.

Ekdale EG (2011) Morphological variation in the ear region of Pleistocene Elephantimorpha (Mammalia, Proboscidea) from Central Texas. *J Morphol* **272**, 452–464.

Ekdale EG (2013) Comparative anatomy of the bony labyrinth (inner ear) of placental mammals. *PLoS ONE* **8**, e66624: 1–100.

Ekdale EG, Rowe T (2011) Morphology and variation within the bony labyrinth of zhelestids (Mammalia, Eutheria) and other therian mammals. *J Vertebr Paleontol* **31**, 658–675.

Elissamburu A (2004) Análisis morfométrico y morfofuncional del esqueleto apendicular de *Paedotherium* (Mammalia, Notoungulata). *Ameghiniana* **41**, 363–380.

Elissamburu A (2012) Estimation of the body mass in the Notoungulata order. *Estudios Geologicós* **68**, 91–111.

Fleischer G (1973) Studien am Skelett des Gehörorgans der Säugetiere, einschließlich des Menschen. *Säugetierkd Mitt* **21**, 131–239.

Flynn JJ, Croft DA, Charrier R, et al. (2005) New Mesotheriidae (Mammalia, Notoungulata, Typotheria), geochronology and tectonics of the Caragua area, northernmost Chile. *J South Am Earth Sci* **19**, 55–74.

Flynn JJ, Charrier R, Croft DA, et al. (2012) Cenozoic Andean faunas: shedding new light on South American mammal evolution, biogeography, environments, and tectonics. In: *Historical Biogeography of Neotropical Mammals* (eds Patterson BD, Costa LP), pp. 51–75. Chicago, IL: University of Chicago Press.

Gabbert SL (2004) The basicranium and posterior cranial anatomy of the families of the Toxodontia. *Bull Am Mus Nat Hist* **285**, 177–190.

Geisler JH, Luo ZX (1996) The petrosal and inner ear of *Herpetocetus* sp. (Mammalia: Cetacea) and their implications for the phylogeny and hearing of archaic mysticetes. *J Paleontol* **70**, 1045–1066.

Gray AA (1907) *The Labyrinth of Animals: Including Mammals, Birds, Reptiles and Amphibians*, Vol. **1**. London: J & A Churchill.

Gray AA (1908) *The Labyrinth of Animals: Including Mammals, Birds, Reptiles and Amphibians*, Vol. **2**. London: J & A Churchill.

Gray H (1977) *Anatomy, Descriptive and Surgical*. Classic collector's edition reprint of revised American from 15th English edn (published 1901). New York: Gramercy Books.

Grothe B, Pecka M, McAlpine D (2010) Mechanisms of sound localization in mammals. *Physiol Rev* **90**, 983–1012.

Hitz R, Flynn JJ, Wyss AR (2006) New basal Interatheriidae (Typotheria, Notoungulata, Mammalia) from the Paleogene of central Chile. *Am Mus Novit* **3520**, 1–32.

Horovitz I (2004) Eutherian mammal systematics and the origins of South American ungulates as based on postcranial osteology. *Bull Carnegie Mus Nat Hist* **36**, 63–79.

Horovitz I, Ladevèze S, Argot C, et al. (2008) The anatomy of *Herpetotherium* cf. *fugax* Cope, 1873, a metatherian from the Oligocene of North America. *Palaeontographica (A)* **284**, 109–141.

Horovitz I, Martin T, Bloch J, et al. (2009) Cranial anatomy of the earliest marsupials and the origin of opossums. *PLoS ONE* **4**, e8278: 1–9.

Hyrtl J (1845) *Vergleichend-anatomische Untersuchungen über das innere Gehörorgan des Menschen und der Säugethiere*. Prague: Friedrich Ehrlich.

Jerison HJ (1971) Quantitative analysis of the evolution of the camelid brain. *Am Nat* **105**, 227–239.

Ladevèze S, Asher RJ, Sánchez-Villagra MR (2008) Petrosal anatomy in the fossil mammal *Necrolestes*: evidence for metatherian affinities and comparisons with the extant marsupial mole. *J Anat* **213**, 686–697.

Lebrun R, de León MP, Tafforeau P, et al. (2010) Deep evolutionary roots of strepsirrhine primate labyrinthine morphology. *J Anat* **216**, 368–380.

Luo ZX, Eastman ER (1995) Petrosal and inner ear of a squalodontoid whale: implications for evolution of hearing in odontocetes. *J Vertebr Paleontol* **15**, 431–442.

Luo ZX, Ketten DR (1991) CT scanning and computerized reconstructions of the inner ear of multituberculate mammals. *J Vertebr Paleontol* **11**, 220–228.

Luo ZX, Marsh K (1996) Petrosal (periotic) and inner ear of a Pliocene kogiine whale (Kogiinae, Odontoceti): implications on relationships and hearing evolution of toothed whales. *J Vertebr Paleontol* **16**, 328–348.

Luo ZX, Ruf I, Schultz JA, et al. (2011) Fossil evidence on evolution of inner ear cochlea in Jurassic mammals. *P Roy Soc B- Biol Sci* **278**, 28–34.

Luo ZX, Ruf I, Martin T (2012) The petrosal and inner ear of the Late Jurassic cladotherian mammal *Dryolestes leiriensis* and implications for evolution of ear in therian mammals. *Zool J Linn Soc* **166**, 433–463.

MacIntyre GT (1972) The trisulcate petrosal pattern of mammals. In: *Evolutionary Biology*, Vol. **6** (eds Dobzhansky T, Hecht MK, Steere WC), pp. 275–303. New York: Appleton-Century-Crofts.

Macrini TE, Flynn JJ, Croft DA, et al. (2010) Inner ear of a notoungulate placental mammal: anatomical description and examination of potentially phylogenetically informative characters. *J Anat* **216**, 600–610.

Madden RH (1997) A new toxodontid notoungulate. In: *Vertebrate Paleontology in the Neotropics: the Miocene Fauna of La Venta, Colombia* (eds Kay RF, Madden RH, Cifelli RL, Flynn JJ), pp. 335–354. Washington, DC: Smithsonian Institution Press.

Maddison WP, Maddison DR (2010) Mesquite: a modular system for evolutionary analysis. Version 2.74 http://mesquiteproject.org.

Manoussaki D, Chadwick RS, Ketten DR, et al. (2008) The influence of cochlear shape on low-frequency hearing. *Proc Natl Acad Sci USA* **105**, 6162–6166.

Marshall LG (1976) Fossil localities for Santacrucian (early Miocene) mammals, Santa Cruz Province, southern Patagonia, Argentina. *J Paleontol* **50**, 1129–1142.

Meng J, Fox RC (1995) Osseous inner ear structures and hearing in early marsupials and placentals. *Zool J Linn Soc* **115**, 47–71.

Nasif NL, Musalem S, Cerdeño E (2000) A new toxodont from the Late Miocene of Catamarca, Argentina, and a phylogenetic analysis of the Toxodontidae. *J Vertebr Paleontol* **20**, 591–600.

Ni X, Flynn JJ, Wyss AR (2010) The bony labyrinth of the early platyrrhine primate *Chilecebus*. *J Hum Evol* **59**, 595–607.

Ni X, Flynn JJ, Wyss AR (2012) Imaging the inner ear in fossil mammals: high-resolution CT scanning and 3-D virtual reconstructions. *Palaeontol Electron* **15**, 18A: 1–10.

O'Leary M, Bloch J, Flynn J, et al. (2013) The placental mammal ancestor and the post-K-Pg radiation of placentals. *Science* **339**, 662–667.

Orliac MJ, Argot C, Gilissen E (2012a) Digital cranial endocast of *Hyopsodus* (Mammalia, 'Condylarthra'): a case of Paleogene terrestrial echolocation? *PLoS ONE* **7**, e30000: 1–10.

Orliac MJ, Benoit J, O'Leary MA (2012b) The inner ear of *Diacodexis*, the oldest artiodactyl mammal. *J Anat* **221**, 417–426.

Patterson B (1932) The auditory region of the Toxodontia. *Field Mus Nat Hist, Geol Ser* **6**, 5–27.

Patterson B (1934a) The auditory region of an upper Pliocene typotherid. *Geol Ser, Field Mus Nat Hist* **6**, 83–89.

Patterson B (1934b) Upper premolar-molar structure in the Notoungulata with notes on taxonomy. *Geol Ser, Field Mus Nat Hist* **6**, 91–111.

Patterson B (1936) The internal structure of the ear in some notoungulates. *Geol Ser, Field Mus Nat Hist* **6**, 199–227.

Patterson B, Pascual R (1968) The fossil mammal fauna of South America. *Q Rev Biol* **43**, 409–451.

Reguero MA, Dozo MT, Cerdeño E (2007) A poorly known rodentlike mammal (Pachyrukhinae, Hegetotheriidae, Notoungulata) from the Deseadan (Late Oligocene) of Argentina. Paleoecology, biogeography, and radiation of the rodentlike ungulates in South America. *J Paleontol* **81**, 1301–1307.

Rougier GW, Wible JR, Novacek MJ (1998) Implications of *Deltatheridium* specimens for early marsupial history. *Nature* **396**, 459–463.

Ruf I, Luo ZX, Wible JR, et al. (2009) Petrosal anatomy and inner ear structures of the Late Jurassic *Henkelotherium* (Mammalia, Cladotheria, Dryolestoidea): insight into the early evolution of the ear region in cladotherian mammals. *J Anat* **214**, 679–693.

Sánchez-Villagra MR, Schmelzle T (2007) Anatomy and development of the bony inner ear in the woolly opossum, *Caluromys philander* (Didelphimorphia, Marsupialia). *Mastozool Neotrop* **14**, 53–60.

Schmelzle T, Sánchez-Villagra MR, Maier W (2007) Vestibular labyrinth diversity in diprotodontian marsupial mammals. *Mammal Study* **32**, 83–97.

Seckel L, Janis C (2008) Convergences in scapula morphology among small cursorial mammals: an osteological correlate for locomotory specialization. *J Mamm Evol* **15**, 261–279.

Segall W (1970) Morphological parallelisms of the bulla and auditory ossicles in some insectivores and marsupials. *Fieldiana Zool* **51**, 169–205.

Shockey BJ (1997) Two new notoungulates (Family Notohippidae) from the Salla Beds of Bolivia (Deseadan: late Oligocene): systematics and functional morphology. *J Vertebr Paleontol* **17**, 584–599.

Shockey BJ, Anaya F (2008) Postcranial osteology of mammals of Salla, Bolivia (late Oligocene): form, function, and phylogenetic implications. In: *Mammalian Evolutionary Morphology: A Tribute to Frederick S. Szalay*. (eds Sargis E, Dagosto M), pp. 135–157. Dordrecht: Springer.

Shockey BJ, Croft DA, Anaya F (2007) Analysis of function in the absence of extant functional homologues: a case study using mesotheriid notoungulates (Mammalia). *Paleobiology* **33**, 227–247.

Shockey BJ, Flynn JJ, Croft DA, et al. (2012) New leontiniid Notoungulata (Mammalia) from Chile and Argentina: comparative anatomy, character analysis, and phylogenetic hypotheses. *Am Mus Novit* **3737**, 1–64.

Silcox MT, Bloch JI, Boyer DM, et al. (2009) Semicircular canal system in early primates. *J Hum Evol* **56**, 315–327.

Silva M, Downing JA (1995) *CRC Handbook of Mammalian Body Masses*. New York: CRC Press.

Simpson GG (1936) Structure of a primitive notoungulate cranium. *Am Mus Novit* **824**, 1–32.

Simpson GG (1948) The beginning of the age of mammals in South America. Part 1. *Bull Am Mus Nat Hist* **91**, 1–232.

Simpson GG (1967) The beginning of the age of mammals in South America. Part 2. *Bull Am Mus Nat Hist* **137**, 1–260.

Simpson GG (1980) *Splendid Isolation: the Curious History of South American Mammals*. New Haven: Yale University Press.

Sinclair WJ (1909) Mammalia of the Santa Cruz beds. Vol. VI. Part I. Typotheria. In: *Reports of the Princeton University Expeditions to Patagonia, 1896–1899*. (ed. Scott WB), pp. 1–110. Lancaster, PA: Lancaster Press.

Spoor F (2003) The semicircular canal system and locomotor behaviour, with special reference to hominin evolution. *Cour Forsch-Inst Senckenberg* **243**, 93–104.

Spoor F, Zonneveld F (1995) Morphometry of the primate bony labyrinth: a new method based on high-resolution computed tomography. *J Anat* **186**, 271–286.

Spoor F, Zonneveld F (1998) Comparative review of the human bony labyrinth. *Yearbk Phys Anthropol* **41**, 211–251.

Spoor F, Garland T, Krovitz G, et al. (2007) The primate semicircular canal system and locomotion. *Proc Natl Acad Sci USA* **104**, 10808–10812.

Townsend B, Croft DA (2010) Middle Miocene mesotheriine diversity at Cerdas, Bolivia, and a reconsideration of *Plesiotypotherium minus*. *Palaeontol Electron* **13**, 1A: 1–36.

Vizcaíno SF, Kay RF, Bargo MS (2012) Background for a paleoecological study of the Santa Cruz Formation (late Early Miocene) on the Atlantic Coast of Patagonia. In: *Early Miocene Paleobiology in Patagonia: High-Latitude Paleocommunities of the Santa Cruz Formation* (eds Vizcaíno SF, Kay RF, Bargo MS), pp. 1–22. Cambridge: Cambridge University Press.

West CD (1985) The relationship of the spiral turns of the cochlea and the length of the basilar membrane to the range of audible frequencies in ground dwelling mammals. *J Acoust Soc Am* **77**, 1091–1101.

Wible JR, Novacek MJ, Rougier GW (2004) New data on the skull and dentition in the Mongolian Late Cretaceous eutherian mammal *Zalambdalestes*. *Bull Am Mus Nat Hist* **281**, 1–144.

Wible JR, Rougier GW, Novacek MJ, et al. (2007) Cretaceous eutherians and Laurasian origin for placental mammals near the K/T boundary. *Nature* **447**, 1003–1006.